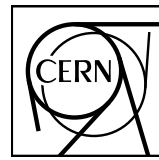


EUROPEAN ORGANIZATION FOR NUCLEAR RESEARCH



ALICE



CERN-EP-2022-126

09 June 2022

 $f_0(980)$ production in inelastic pp collisions at $\sqrt{s} = 5.02$ TeV

ALICE Collaboration*

Abstract

The measurement of the production of $f_0(980)$ in inelastic pp collisions at $\sqrt{s} = 5.02$ TeV is presented. This is the first reported measurement of inclusive $f_0(980)$ yield at LHC energies. The production is measured at midrapidity, $|y| < 0.5$, in a wide transverse momentum range, $0 < p_T < 16$ GeV/ c , by reconstructing the resonance in the $f_0(980) \rightarrow \pi^+ \pi^-$ hadronic decay channel using the ALICE detector. The p_T -differential yields are compared to those of pions, protons and ϕ mesons as well as to predictions from the HERWIG 7.2 QCD-inspired Monte Carlo event generator and calculations from a coalescence model that uses the AMPT model as an input. The ratio of the p_T -integrated yield of $f_0(980)$ relative to pions is compared to measurements in $e^+ e^-$ and pp collisions at lower energies and predictions from statistical hadronisation models and HERWIG 7.2. A mild collision energy dependence of the $f_0(980)$ to pion production is observed in pp collisions from SPS to LHC energies. All considered models underpredict the p_T -integrated $2f_0(980)/(\pi^+ + \pi^-)$ ratio. The prediction from the canonical statistical hadronisation model assuming a zero total strangeness content of $f_0(980)$ is consistent with the data within 1.9σ and is the closest to the data. The results provide an essential reference for future measurements of the particle yield and nuclear modification in p–Pb and Pb–Pb collisions, which have been proposed to be instrumental to probe the elusive nature and quark composition of the $f_0(980)$ scalar meson.

© 2022 CERN for the benefit of the ALICE Collaboration.

Reproduction of this article or parts of it is allowed as specified in the CC-BY-4.0 license.

*See Appendix A for the list of collaboration members

1 Introduction

The conventional picture for the classification of hadrons is based on the constituent quark model introduced in the 1960s [1], in which the observed mesons and baryons are described as colourless q̄q and qq̄ bound states, respectively. Most of the known observed states fit into the quark model picture. At the same time, there are states whose quantum numbers are known but their mass and width have not been measured, and observed resonances whose properties suggest an exotic structure [2]. One remarkable case is that of the light scalar mesons, light-flavoured states with spin zero, positive parity and charge ($J^{PC} = 0^{++}$) and masses below 2 GeV/ c^2 , whose identification represents a long-standing puzzle in particle physics [3–8]. From a theoretical point of view, the structure of these states is highly debated [2]: light scalar mesons could be conventional q̄q mesons, or compact (qq)(q̄q) structures (tetraquarks), or meson–meson bound states in the form of hadronic molecules, or a superposition of all these components, or glueballs.

From an experimental point of view, light scalar resonances are typically reconstructed via their dominant decay channels into pseudoscalar mesons (e.g., $\pi\pi$, $\eta\pi$, $\eta\eta$...). The states decaying into pions, in particular, have large characteristic decay widths, of the order of few tens to few hundreds of MeV/ c^2 , due to the large available phase space. Therefore, the isolation of the particle signals is particularly challenging as broad signals strongly overlap. In addition, for some of the scalar meson states, different decay channels can open up within a short mass interval and distort the line shapes of the nearby resonances.

Among the scalar mesons, the f₀(980) state is particularly interesting for two reasons. First, despite a long history of experimental and theoretical studies, its nature is still controversial as the properties of the f₀(980) state are compatible with a conventional q̄q meson [9], a tetraquark [10], and a K̄K molecular [11] structure. Secondly, the f₀(980) represents an interesting probe of the high-density hadronic final state of heavy-ion collisions and in-medium particle formation mechanisms [12].

The f₀(980) couples predominantly to the $\pi\pi$ and K̄K channels and its signal overlaps strongly with the background represented mainly by the f₀(500) and the f₀(1370), among the scalar mesons. An indication in favour of the tetraquark structure of f₀(980) [13] comes from measurements of the ϕ meson radiative decay branching ratios by SND [14], CMD2 [15], and KLOE [16, 17] experiments. This is further supported by a recent analysis [10] of the J/ψ radiative decay data from BESIII [10, 18]. The f₀(980) is also prominently produced in D_s⁺ decays as reported by the E791 collaboration [19], and observed in weak decays of B and B_s mesons measured with LHCb [20, 21]. There, the appearance of the f₀(980) in competition with the ϕ meson in these decays could be explained by a large s̄s component of this state, combined with the fact that the c → s coupling is Cabibbo favoured. In this scenario, the structure of the f₀(980) would be $|f_0(980)\rangle = |(u\bar{u} + d\bar{d})s\bar{s}\rangle/\sqrt{2}$ [2]. An analysis of the measured couplings of the B and B_s mesons to $J/\psi + f_0(980)$ excluded the tetraquark hypothesis [21], a conclusion that is however challenged by a different analysis of the same data [22]. Indications that f₀(980) could be a K̄K molecule come instead from the study of pion–pion and kaon–kaon scattering via non-perturbative QCD methods, which use effective meson-exchange models of the $\pi\pi$ interaction [23, 24] and study the K̄K interaction for coupled and single channels in chiral effective theory [11, 25].

In addition to measuring the production rates and branching fractions of f₀(980) in ϕ and heavy-flavour decays, several authors [7, 26–28] have proposed to investigate its nature by using heavy-ion collisions and exploiting the unique production (and decay) environment accessible in these reactions. In high-energy heavy-ion collisions, two extreme states of matter are reached one after the other. If enough energy is deposited in the collision region, the state of deconfined strongly interacting matter called quark–gluon plasma (QGP) is produced and expands as a nearly perfect liquid until the temperature reaches the pseudo-critical value of ≈ 155 MeV [29] and a transition to confined QCD matter takes place. A hot (T ≈ 100–150 MeV) and dense gas of interacting hadrons is formed in which resonances decay and particles interact (pseudo)elastically until they decouple. At the LHC, the system produced

in Pb–Pb collisions decouples after about 10 fm/c [30] and the production of hadronic resonances with lifetimes of the order of 1 to 10 fm/c is studied to characterise the hadronic stage of the collision [31–33]. With its width between 10 and 100 MeV/c² and a corresponding lifetime of \approx 5–10 fm/c, the f₀(980) is a probe for the dense hadron gas formed in the late stage of heavy-ion collisions [12].

Measurements of the nuclear modification factor [26], the particle yield per event [27], and the elliptic flow coefficient [28] have been suggested to provide insights into the internal structure of the f₀(980). Models of hadron formation via recombination (coalescence) [34–36] of quarks in the quark–gluon plasma that have been successful in describing LHC data, indicate that the f₀(980) production in the intermediate transverse momentum range ($2 < p_T < 5$ GeV/c) is sensitive to the number of constituent quarks. Theory calculations based on a coalescence model [27] show that the p_T -integrated production of f₀(980) in central heavy-ion collisions at LHC energies is expected to be two orders of magnitude lower if the state has a tetraquark structure compared to the results for a non-exotic diquark structure q \bar{q} , or a hadronic molecule configuration. On the other hand, the production of a tetraquark state would be enhanced in heavy-ion collisions with respect to pp collisions at the same energy in the \approx 2–6 GeV/c momentum range [7, 26]. Measurements of the nuclear modification factor [7, 26] or of the p_T -dependent yield ratio of the f₀(980) to particles with different (but established) quark content could therefore shed light on the nature of the state. The authors of [28] also suggest that the azimuthal production asymmetry in the f₀(980) momentum distributions, quantified by the elliptic flow coefficient, could be sensitive to the number of constituent quarks in the kinematic range in which hadron formation occurs predominantly via quark recombination (coalescence). A measurement of the f₀(980) production in pp collisions is necessary for the determination of the nuclear modification factor and constitutes a reference for the study of the particle production in heavy-ion collisions.

In this letter, the first measurement of the inclusive production of f₀(980) in inelastic pp collisions at the LHC is reported. To provide a baseline for studies in heavy-ion interactions, the data using collisions at $\sqrt{s} = 5.02$ TeV were analysed, corresponding to the centre-of-mass energy per nucleon pair of the p–Pb and Pb–Pb data samples collected during the LHC Run 2. Measurements of f₀(980) in p–Pb and Pb–Pb collisions at this energy will be the subject of future publications. The production of f₀(980) is measured at midrapidity, $|y| < 0.5$, in a broad transverse momentum range between 0 and 16 GeV/c. An overview of the ALICE experimental setup is given in Sec. 2, followed by a description of the analysis strategy in Sec. 3. This includes details on the data sample, the f₀(980) signal reconstruction, the yield extraction and corrections, and the systematic uncertainty estimation. Results are discussed in comparison to lower energy data and theoretical models in Sec. 4, while in Sec. 5 the conclusions are summarised.

2 Experimental setup

The experimental setup and details on the performance of the ALICE detector are described in Refs. [37, 38]. The ALICE detector consists of a central barrel with a set of detectors devoted to the reconstruction and identification of the charged particles, a forward muon spectrometer and a set of backward and forward systems for triggering and event characterisation purposes. The central barrel detectors are located inside a solenoidal magnet that provides a magnetic field of 0.5 T. The main detectors employed for the analysis presented in this work are the V0, the Inner Tracking System (ITS), the Time Projection Chamber (TPC), and the Time-of-Flight detector (TOF). The V0 consists of two scintillator arrays placed on both sides of the interaction point covering the pseudorapidity regions $2.8 < \eta < 5.1$ (V0A) and $-3.4 < \eta < -1.7$ (V0C), respectively. The V0 provides the minimum bias trigger of the experiment and is used for suppressing beam-induced background at the offline analysis level. The position of the collision vertex and the tracks of charged particles are reconstructed in the central barrel using the ITS and the TPC. The ITS is a high-resolution tracker that consists of six cylindrical layers of silicon detectors. The TPC is a large cylindrical drift detector covering a radial distance of $85 < r < 247$ cm from the beam axis and having longitudinal dimensions of about $-250 < z < 250$ cm. The TOF is a large

area array of multigap resistive plate chambers, placed at a radius of about 370–399 cm from the beam line. In the central barrel, charged particles can be identified via measurements of their specific energy loss, dE/dx , provided by the TPC with a resolution of 5%, and via their time-of-flight measured by the TOF with a resolution of about 80 ps.

3 Data analysis

The measurement of f₀(980) production is performed using a sample of minimum bias pp collision events at a centre-of-mass energy of $\sqrt{s} = 5.02$ TeV, collected in the years 2015 and 2017. The minimum-bias trigger requires at least one hit in both V0A and V0C detectors [39]. The integrated luminosity after trigger selection is $\approx 21.8 \text{ nb}^{-1}$. Events are selected for the analysis if the position of the reconstructed collision vertex along the beam axis is located within 10 cm from the nominal interaction point. To reduce the pileup caused by multiple interactions in the same bunch crossing, a criterion based on the offline reconstruction of multiple primary vertices in the two innermost layers of the ITS, namely the Silicon Pixel Detector (SPD) is applied [37]. The rejected events account for less than 1% of the total events. After applying these selection criteria, $\approx 9.14 \times 10^8$ collision events have been analysed.

The f₀(980) resonance signal is reconstructed via its decay into a pair of oppositely charged pions, $f_0(980) \rightarrow \pi^+ \pi^-$. This requires the reconstruction, selection and identification of pion tracks in the central barrel of ALICE. To ensure a uniform detector acceptance, only charged tracks with $p_T > 0.15 \text{ GeV}/c$ and pseudorapidity $|\eta| < 0.8$ are considered for the analysis. Track selection criteria are applied to the charged tracks as in previous works [31, 32] to ensure a good quality of the reconstruction. To this end, each track in the TPC is required to have crossed at least 70 readout pad rows out of a maximum possible 159. To reduce the contamination from secondary particles, tracks are accepted if their distance of closest approach to the collision vertex in the longitudinal (d_z) and transverse (d_{xy}) directions satisfy $d_z < 2$ and $d_{xy} < 0.0105 + 0.0350 \times p_T^{-1.1}$, where p_T and distance are in units of GeV/c and cm, respectively.

The identification of pions is performed using the TPC and the TOF detectors and criteria based on the difference between the measured and expected signals for a given particle hypothesis, divided by the resolution (σ_{TPC} , σ_{TOF}). In the TPC, charged particles are identified as π if the measured dE/dx is compatible with the expected pion mean specific energy loss within two standard deviations ($2\sigma_{\text{TPC}}$) over the entire momentum range. If a measurement of the particle time-of-flight by the TOF is available, a TOF-based $3\sigma_{\text{TOF}}$ selection criterion is applied on top of the TPC-based one, over the measured momentum range.

3.1 Raw yield extraction

The f₀(980) resonance signal is reconstructed via an invariant mass analysis by combining oppositely-charged pions within the same event into pairs and imposing the pair to have a rapidity within the range $|y| < 0.5$. To remove the combinatorial background, the like-sign method is employed. The same-charge pion tracks from the same event are combined into $\pi^+ \pi^+$ and $\pi^- \pi^-$ pairs. The total like-sign invariant mass distribution is calculated as the geometric mean of the positively-charged and negatively-charged pair distributions, as $2\sqrt{N^{++}N^{--}}$, where N^{++} and N^{--} are the number of $\pi^+ \pi^+$ and $\pi^- \pi^-$ pairs, respectively. The $\pi^+ \pi^-$ and like-sign background invariant mass distributions are extracted for various intervals of the pair p_T , and for each of these, the like-sign background is subtracted from the unlike-sign pair distribution. After the subtraction of the combinatorial background, the f₀(980) signal peak, sitting on the right-hand tail of the broad $\rho(770)$ meson signal, is visible on top of a residual background. Two examples of the $\pi^+ \pi^-$ invariant mass distributions after combinatorial background subtraction are shown in Fig. 1 for a low- p_T and for a high- p_T interval. With increasing p_T , the significance of the f₂(1270) resonance signal increases and the broad f₂(1270) peak becomes visible on the right side of the f₀(980) signal. The residual background originates from correlated $\pi^+ \pi^-$ pairs from mini-jets and from

misidentified particles. The main contributions to the correlated background arise from the decay of the $\rho(770)$ and the $f_2(1270)$ resonances into oppositely-charged π pairs. In order to extract the $f_0(980)$ yields in each p_T interval, the distributions are fitted in the invariant mass interval $0.8 < M_{\pi\pi} < 1.6 \text{ GeV}/c^2$ with a function that is the sum of three relativistic Breit-Wigner functions (rBW) describing the $\rho(770)$, $f_0(980)$ and $f_2(1270)$ signals [31, 40, 41], and a residual background. Since the resolution on the invariant mass is negligible with respect to the natural width of the considered resonances, the resonance shape can be modelled with a rBR with no need for any additional Gaussian smearing to account for detector resolution effects. Each of the rBW functions is defined as

$$\text{rBW}(M_{\pi\pi}) = \frac{AM_{\pi\pi}\Gamma(M_{\pi\pi})M_0}{(M_{\pi\pi}^2 - M_0^2)^2 + M_0^2\Gamma^2(M_{\pi\pi})} \quad (1)$$

where $\Gamma(M_{\pi\pi})$ is given by

$$\Gamma(M_{\pi\pi}) = \left[\frac{(M_{\pi\pi}^2 - 4m_\pi^2)}{(M_0^2 - 4m_\pi^2)} \right]^{(2J+1)/2} \times \frac{\Gamma_0 M_0}{M_{\pi\pi}}. \quad (2)$$

Here, A is the normalisation constant, M_0 and Γ_0 are the rest mass and width of the resonance, m_π is the charged pion mass and the spin is $J = 0$ for $f_0(980)$, $J = 1$ for $\rho(770)$ and $J = 2$ for $f_2(1270)$. The shape of the residual background resembles that of a Maxwell-Boltzmann distribution and therefore it is fitted with a similar functional form $f_{\text{bg}}(M_{\pi\pi})$

$$f_{\text{bg}}(M_{\pi\pi}) = B\sqrt{(m_{\pi\pi} - m_{\text{cutoff}})^n} C^{3/2} \exp[-C(m_{\pi\pi} - m_{\text{cutoff}})^n], \quad (3)$$

where B is the normalisation constant and m_{cutoff} is the low-mass cutoff expected to be equal to the rest mass of the $\pi^+\pi^-$ pair. This function was proven to provide a good description of the residual background in previous analyses [33]. The residual background term takes also into account any possible additional background from $f_0(500)$ and $f_0(1370)$, which have not been added to the signal model due to the large indetermination¹ on the broad width parameter of these states.

For the extraction of the particle yields, the fits are performed with the following configuration of the fit parameters. The mass and the width of the $\rho(770)$, and the width of the $f_2(1270)$ are fixed to their vacuum values, $m_\rho = 775.26 \text{ MeV}/c^2$, $\Gamma_\rho = 149.1 \text{ MeV}/c^2$, and $\Gamma_{f_2} = 186.7 \text{ MeV}/c^2$ [2]. The width of the $f_0(980)$ is fixed to the average value of the range reported in Ref. [2] that corresponds to $\Gamma_{f_0} = 0.055 \text{ GeV}/c^2$. The masses of the $f_0(980)$ and the $f_2(1270)$, as well as the m_{cutoff} , C and n parameters of f_{bg} are left free. The fit parameter configuration has been varied to take into account possible imperfections in the description of the background and signal shapes, as discussed in Section 3.3. In Fig. 1, the fit result to the invariant mass distribution of $\pi^+\pi^-$ pairs after like-sign background subtraction is shown for two p_T intervals, namely $0.6 < p_T < 0.8 \text{ GeV}/c$ and $5 < p_T < 6 \text{ GeV}/c$.

3.2 Yield corrections

In order to obtain the $f_0(980)$ production yield per unit of rapidity and p_T per inelastic event ($\frac{1}{N_{\text{INEL}}} \frac{d^2N}{dy dp_T}$), several correction factors are applied to the raw yields obtained from the fit procedure in each p_T interval according to the following formula

$$\frac{1}{N_{\text{INEL}}} \frac{d^2N}{dp_T dy} = \frac{1}{N_{\text{evt}}} \frac{N_{f_0(980) \rightarrow \pi\pi}}{\Delta p_T \Delta y} \frac{\epsilon_{\text{trig}} \epsilon_{\text{vtx}} f_{\text{sig}}}{A \times \epsilon_{\text{rec}} \text{BR}}. \quad (4)$$

Here, $N_{f_0(980) \rightarrow \pi\pi}$ is the $f_0(980)$ raw yield measured in a given rapidity (Δy) and transverse momentum (Δp_T) interval, N_{evt} is the number of collision events that satisfy the selection criteria. The minimum-bias

¹The $f_0(500)$ width ranges from 400 to 700 MeV, the $f_0(1370)$ width ranges from 200 to 500 MeV [2]

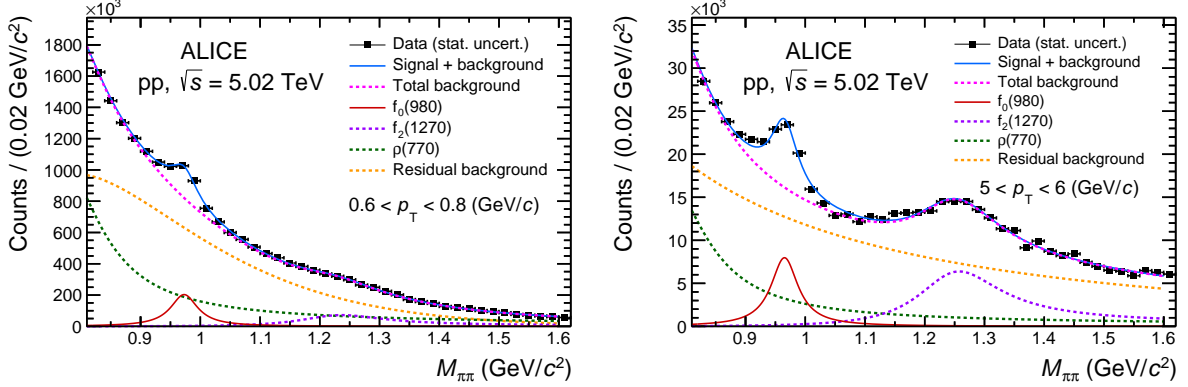


Figure 1: Left (right) plot shows the invariant mass distribution of $\pi^+\pi^-$ pairs after like-sign background subtraction in low (high) transverse-momentum interval in pp collisions at $\sqrt{s} = 5.02$ TeV in $|y| < 0.5$. Solid blue curves represent fits with the function shown in Eq. 1 and a residual background shown in Eq. 3. Solid red curve represents $f_0(980)$ signal while other dashed curves represent the background contributions from $\rho(770)$, $f_2(1270)$ and residual background.

trigger efficiency, the vertex reconstruction efficiency and the signal loss correction factor are represented by $\varepsilon_{\text{trig}}$, ε_{vtx} and f_{sig} , respectively. The branching ratio correction amounts to $\text{BR} = (46 \pm 6)\%$ [42] assuming dominance of $\pi\pi$ and KK channels. The yields of $f_0(980)$ are normalised to the number of inelastic pp collisions with a trigger efficiency correction, $\varepsilon_{\text{trig}} = 0.757 \pm 0.019$ [43, 44], which takes into account the efficiency of the V0-based trigger to select inelastic events. The vertex reconstruction efficiency in pp collisions at $\sqrt{s} = 5.02$ TeV is found to be $\varepsilon_{\text{vtx}} = 0.958$ [32]. The $A \times \varepsilon_{\text{rec}}$ factor corrects for the detector acceptance times the $f_0(980)$ reconstruction efficiency and is evaluated using a detailed Monte Carlo simulation of the ALICE detector geometry, material, and response. The pp collision events are simulated using the PYTHIA 8 event generator [45] with the addition of the $f_0(980)$ signals. The generated particles in the simulation are propagated through the detector using GEANT3 [46]. The $A \times \varepsilon_{\text{rec}}$ is calculated in the rapidity range $|y| < 0.5$ as a function of p_T and is defined as the ratio of the number of reconstructed and generated $f_0(980)$. The reconstruction of $f_0(980)$ in the simulation is performed using the same event and track selection criteria as employed for the analysis of the data. The signal loss correction factor, f_{sig} , accounts for the fraction of $f_0(980)$ signal lost due to trigger inefficiencies and can be determined as a function of p_T using Monte Carlo simulations. Because a simulation with injected $f_0(980)$ signals may not lead to a realistic estimate of this correction factor, the correction is taken to be the same as for the ϕ meson at the same collision energy. The earlier analysis in [32] showed that this correction does not depend significantly on the particle mass for resonances decaying strongly into two charged particles. This factor ranges between 1.07 for $0 < p_T < 0.2$ GeV/c and 1 for $p_T > 2.5$ GeV/c .

3.3 Systematic uncertainties

The sources of systematic uncertainty in the measurement of the $f_0(980)$ yields are summarised in Table 1. These include yield extraction, track and event selection, global tracking efficiency, particle identification, the knowledge of the ALICE material budget, and that of the hadron interaction cross section in the detector material. The estimated values of the uncertainties are reported in Table 1 for low, intermediate and high- p_T intervals. The systematic uncertainty associated with the yield extraction arises from the fit procedure and is determined by varying the fitting range as well as the signal and the background fit parameters. In particular, the width of the $f_0(980)$ was varied by sampling the range from 10 to 100 MeV/c^2 given in [2] with 15 variations and the width of the $f_2(1270)$ was varied within ± 7.5 MeV/c^2 that corresponds to a $\pm 3\sigma$ range of the width value reported in [2]. These variations result in the largest

Table 1: Contributions to the relative systematic uncertainty of the p_T -dependent yield of f₀(980) in pp collisions at $\sqrt{s} = 5.02$ TeV. The uncertainties are given for the lowest and the highest p_T intervals of the measured spectrum as well as for one intermediate p_T interval. The total uncertainty is obtained as the sum in the quadrature of the individual contributions. Values are expressed in percentage (%).

Source of uncertainty	p_T (GeV/c)		
	0–0.2	4–4.5	12–16
Yield extraction	7.1%	8.8%	15.3%
Track selection	9.3%	2.2%	2.1%
Global tracking efficiency	2%	4%	4%
Particle identification	6.8%	1.5%	6%
Event selection	7.6%	2.1%	3.3%
Material budget	5.2%	0%	0%
Hadronic interaction	3.4%	0%	0%
Total	16.8%	10.2%	17.4%

contribution to the uncertainty on the yield extraction. The uncertainties due to the yield extraction are p_T dependent and vary from 7.1% in the lowest p_T interval, to 15.3% in the highest p_T interval of this analysis. The systematic uncertainty due to the track selection is evaluated by varying a single track selection criterion at a time in both data and simulation, and by repeating all the steps of the analysis. This contribution ranges from 9.3% to 2.1% from low to high p_T . The difference in the efficiency of the matching of TPC tracks to ITS clusters (global tracking efficiency) between data and simulations results in a contribution to the systematic uncertainty of 2–4% depending on p_T . The systematic uncertainty associated with the particle identification is due to an imperfection in the description of the dE/dx in the TPC-based $n\sigma$ selection in the Monte Carlo simulation as compared to data. The $n\sigma$ selection is varied in data and simulation simultaneously to a $3\sigma_{\text{TPC}}$ particle identification criterion and results in a p_T -dependent relative systematic uncertainty of 1.5–6.8%. The choice of the event selection criteria leads to a systematic uncertainty of 2.1–7.6%. The systematic uncertainty associated with the signal loss correction is estimated by comparing the correction for ϕ mesons, used as a proxy for f₀(980), with that of other light-flavour hadrons and is found to be lower than 1%. Finally, the uncertainty on the knowledge of the ALICE material budget and that of the hadron interaction cross section in the detector material leads to a systematic uncertainty lower than 5.3% and 3.4%, respectively [38, 47, 48]. The total relative systematic uncertainty is obtained as the sum in the quadrature of these contributions.

4 Results and Discussion

The p_T -differential yield of f₀(980) for $|y| < 0.5$ in inelastic pp collisions at $\sqrt{s} = 5.02$ TeV is shown in the upper panel of Fig. 2. The measurement spans a wide p_T range from 0 to 16 GeV/c.

The normalisation and branching ratio relative uncertainties on the yields are independent of p_T and amount to 2.5% and 13%, respectively [42, 44].

At present, most of the Monte Carlo generators commonly employed to simulate pp collisions do not implement the generation of f₀(980) in their default configurations. One notable exception is the HERWIG 7.2 event generator [49, 50]. HERWIG 7.2 is a QCD-inspired Monte Carlo event generator that includes processes like initial and final state QCD radiation, a description of the underlying event via an eikonal multiple parton–parton interaction model, and a cluster hadronisation model for the formation of hadrons from the quarks and gluons produced in the parton shower. The default hadronisation and shower parameters are tuned to e⁺e[−] data [50] with the addition of a tune for multi-parton processes based on the minimum bias LHC data [49]. To allow for the comparison, model calculations have been performed in the same p_T intervals of the data. As shown in the HERWIG/Data ratio reported in the middle panel

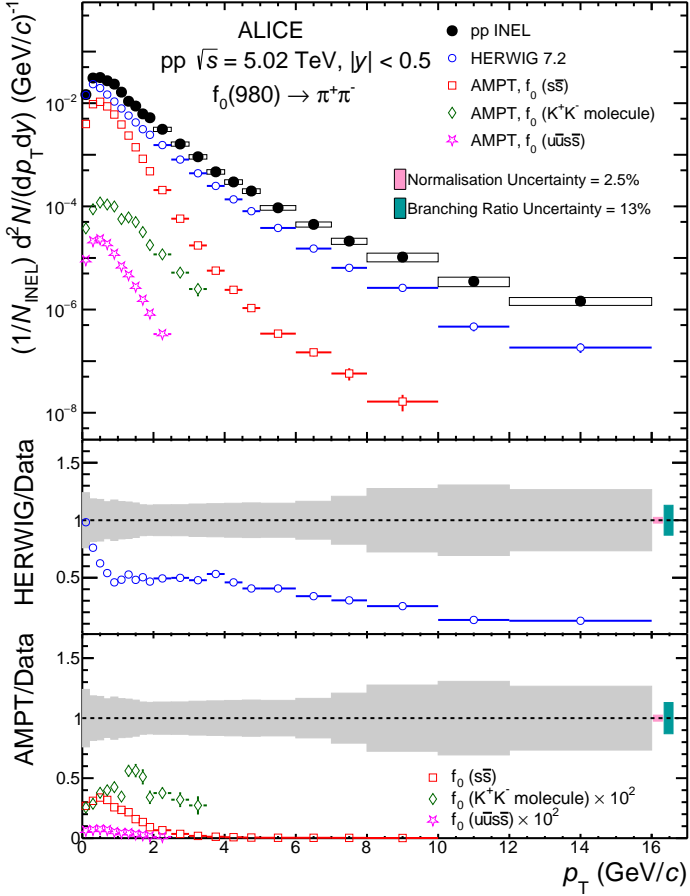


Figure 2: The p_T -differential yield of $f_0(980)$ in pp collisions at $\sqrt{s} = 5.02$ TeV is compared with predictions from the HERWIG 7.2 event generator [49, 50] and with a coalescence calculation [28] based on the AMPT model [51]. The statistical and systematic uncertainties on data (full black markers) are shown as bars and boxes, respectively. The middle and bottom panels show the model to data ratios. The grey boxes at unity represent the sum in quadrature of the statistical and systematic uncertainty on the data. The ratios of $u\bar{u}s\bar{s}$ tetraquark and K^+K^- molecule configurations from AMPT model predictions to data are multiplied by 100 to improve visibility. In all three panels, the uncertainties associated with the models are statistical ones.

of Fig. 2, HERWIG underestimates the measured yields by a factor of about two for $1 < p_T < 4$ GeV/c but reproduces at least qualitatively the shape of the p_T spectrum in this range. At $p_T \lesssim 0.5$ GeV/c, the model is consistent with data within uncertainty but the p_T dependence is not described. At $p_T \geq 4$ GeV/c, HERWIG is not able to reproduce the data neither qualitatively nor quantitatively.

The data are also compared to a recent coalescence calculation [28, 51] that uses the AMPT multiphase transport model [51], coupled with a coalescence afterburner with Gaussian Wigner function to generate $f_0(980)$ in three configurations, i.e., as a $s\bar{s}$ meson, as a $u\bar{u}s\bar{s}$ tetraquark state, and as a K^+K^- molecule. The AMPT model contains four main components namely initial conditions, partonic interactions, conversion from partonic to hadronic matter, and interactions among hadrons based on a relativistic transport (ART) model [52, 53]. The initial conditions are obtained from the HIJING model [54] and the partonic interactions are determined according to the Zhang's Parton Cascade model [55]. In [28], the authors use the phase-space information of quarks from this stage to implement quark coalescence for the $f_0(980)$ with the $s\bar{s}$ and tetraquark configurations. In the default version of AMPT, the conversion of partons to

hadrons is then calculated with the Lund string fragmentation [56–58], while in the string melting version of the model [59], a quark coalescence approach is used to combine partons to form hadrons. The phase-space information of kaons generated at this stage by AMPT is used as input for the coalescence afterburner for the f₀(980) molecular state. As shown in Fig. 2, the s̄s calculation underestimates the f₀(980) p_T distribution by a factor of about three, whereas the molecule and the tetraquark configuration predictions are two and three orders of magnitude lower, respectively. Note that the molecule and the tetraquark configuration prediction ratios to data are reported in the lowest panel of Fig. 2 multiplied by a factor of 100 to improve the visibility. In addition, the shape of the p_T spectra for the s̄s and the ūs̄s̄ tetraquark configurations are found to be significantly steeper than the measured one. Instead, the ratio between the model prediction for the K⁺K⁻ molecule configuration and the data exhibits a milder p_T dependence within uncertainties in the considered p_T range (0–3.5 GeV/c), indicating that in this configuration the model can reproduce qualitatively better the measured spectral shape. Recent theoretical calculations that investigate the inclusive f₀(980) production according to the colour-singlet gluon-gluon fusion and colour evaporation model have been proposed by the authors of [60]. As these exploratory studies are currently available only for $\sqrt{s} = 7$ TeV, a comparison with the data presented in this letter is auspicious in the near future.

The per-event p_T -integrated yield, dN/dy, and average transverse momentum, $\langle p_T \rangle$, are calculated by integrating the p_T -differential yield in the measured transverse momentum range. The obtained values are the following:

$$\frac{dN}{dy} = 0.0385 \pm 0.0001(\text{stat.}) \pm 0.0047(\text{syst.}) \quad (5)$$

$$\langle p_T \rangle = 0.9624 \pm 0.0014(\text{stat.}) \pm 0.0357(\text{syst.}) \text{ GeV}/c \quad (6)$$

Notably, the yield for $p_T > 16$ GeV/c has a negligible contribution to the dN/dy and thus no extrapolation was employed.

The production of f₀(980) is compared to that of other light-flavour hadrons in Fig. 3 where the ratios of the f₀(980) yield to those of $\pi^+ + \pi^-$ [61], p+̄p [61], and ϕ [32] measured in pp collisions at $\sqrt{s} = 5.02$ TeV are reported as a function of p_T . The ratio to $\pi^+ + \pi^-$ mesons exhibits an increasing trend as a function of p_T at low p_T and for $p_T > 5$ GeV/c it saturates within uncertainties.

The comparison of the production of f₀(980) to that of protons and of the ϕ meson is particularly interesting as these particles have similar masses [2] but different quark content. In particular, the ϕ meson is a pure s̄s state, while the f₀(980) contains a light flavour component (ūu, d̄d) as well as a large s̄s component, as suggested by measurements of f₀(980) produced in D_s⁺ decays [19]. The f₀(980) to p+̄p ratio shows an increasing monotonic trend as a function of p_T , whereas the f₀(980) to ϕ ratio decreases for $p_T < 1.5$ GeV/c, remains flat till $p_T \simeq 8$ GeV/c, and increases for $p_T > 8$ GeV/c.

The measured p_T -differential particle yield ratios are compared in Fig. 3 to the predictions from the HERWIG 7.2 event generator. The shape of the measured 2f₀(980)/($\pi^+ + \pi^-$) ratio is fairly well reproduced over almost the entire measured p_T range, although the yield is underestimated by about a factor of two by the model. The model underestimates the 2f₀(980)/(p+̄p) ratio and fails to reproduce its p_T -dependence, with the measured ratio being more steeply increasing with p_T than the predicted one. The trend of f₀(980)/ ϕ ratio is flat for $1 < p_T < 10$ GeV/c suggesting that its p_T dependence is qualitatively well reproduced by HERWIG in this momentum interval. However, the model overestimates the ratio by nearly a factor of two. For $p_T < 1$ GeV/c, the f₀(980)/ ϕ ratio exhibits a steeply decreasing trend, that is qualitatively present also in the model prediction. At high p_T , the HERWIG predictions are consistent with the f₀(980)/ ϕ data within the uncertainties.

The ratio of the p_T -integrated f₀(980) yield relative to pions in pp collisions at $\sqrt{s} = 5.02$ TeV amounts to $2f_0/(\pi^+ + \pi^-) = (0.0186 \pm 0.0026)$, with the uncertainty being the sum in quadrature of the statis-

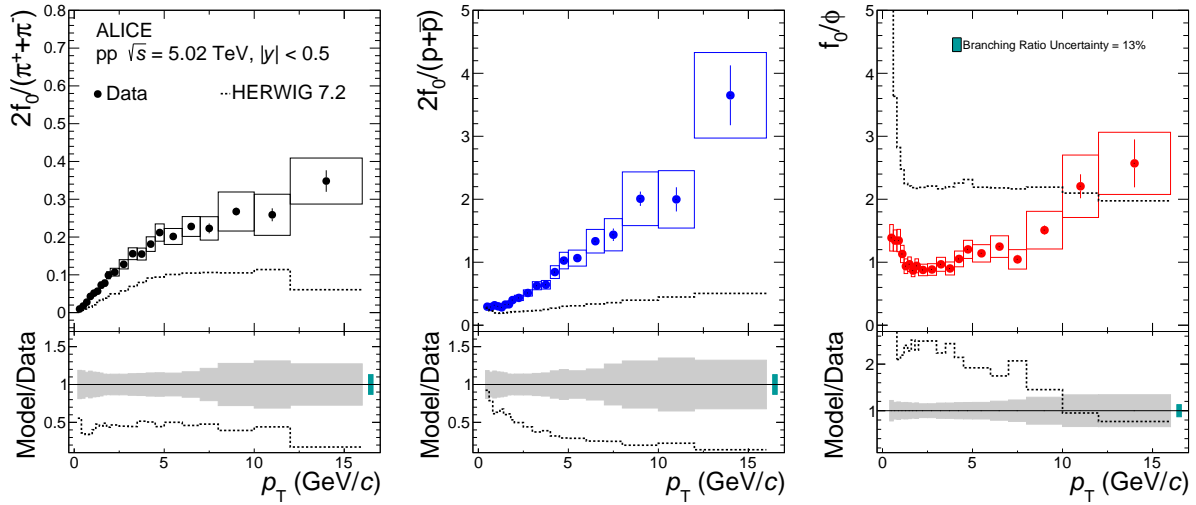


Figure 3: (Upper panels) Particle yield ratios of $f_0(980)$ to $\pi^+ + \pi^-$ [61] (left panel), $p + \bar{p}$ [61] (middle panel), and ϕ [32] (right panel) measured in inelastic pp collisions at $\sqrt{s} = 5.02$ TeV as a function of p_T . Data are compared to HERWIG 7.2 model predictions. The statistical and systematic uncertainties are shown as bars and boxes, respectively. (Lower panels) Ratio of measured particle ratios to the HERWIG model calculations (dashed histogram). The grey boxes at unity represent the sum in quadrature of the statistical and systematic uncertainty on the data. In the right panel, the ratio in the region for $p_T < 0.8$ GeV/c is off-scale. The relative uncertainty of 13% due to the branching ratio correction [42] is shown as a green box with an arbitrary horizontal width for visibility.

tical and systematic uncertainties. The value is shown in Fig. 4 (red point) in comparison with results from measurements in pp and e^+e^- collisions at lower centre-of-mass energies as well as with model calculations.

The low energy experiment results were originally reported using different branching ratios, therefore all of them have been updated to take into account the most recent value of 46% [42] used in this letter. In Fig. 4, the same uncertainty on the BR is applied to all data points and reported as a shaded yellow box. The particle ratio value from the fixed-target NA27 experiment at the CERN SPS, measured in pp collisions at $\sqrt{s} = 27.5$ GeV [64] is 44.5% lower than the ratio measured at $\sqrt{s} = 5.02$ TeV, suggesting a mild increase of the $f_0(980)$ yield relative to pions with increasing energy of the pp collisions. The particle ratio values from e^+e^- collisions at $\sqrt{s} = 29$ GeV [62] and $\sqrt{s} = 91$ GeV [63] are lower by 61% and higher by a factor of two, respectively. The particle ratios are compared with predictions based on statistical hadronisation models [65–67] and the HERWIG 7.2 event generator. The statistical hadronisation model predictions by Becattini et al. for the e^+e^- case [65] and for the pp collisions [66] case underestimate the measurement by about a factor of two, similarly to a Grand Canonical formulation of the statistical hadronisation model (GC-SHM) from the GSI-Heidelberg group [67]. The value from HERWIG is also a factor of about two lower than the measured ratio.

In Fig. 5, the measured p_T -integrated $2f_0/(\pi^+ + \pi^-)$ ratio in pp collisions at $\sqrt{s} = 5.02$ TeV is compared to predictions based on the canonical statistical hadronisation model (CSM) described in [68], as a function of the multiplicity of particles produced in the collision, expressed in terms of the average pseudorapidity density of charged particles, $\langle dN_{ch}/d\eta \rangle$. The prediction spans a large $\langle dN_{ch}/d\eta \rangle$ interval, reaching the high multiplicity achieved in central heavy-ion collisions at LHC energies. In canonical statistical hadronisation models, hadrons are formed from a source that is assumed to have reached full chemical equilibrium at the chemical freeze-out temperature T_{ch} , and their yields are determined from the partition function for a canonical ensemble. The multiplicity dependence of hadron production is driven by the canonical suppression, namely the exact conservation of baryon number, electric charge, and

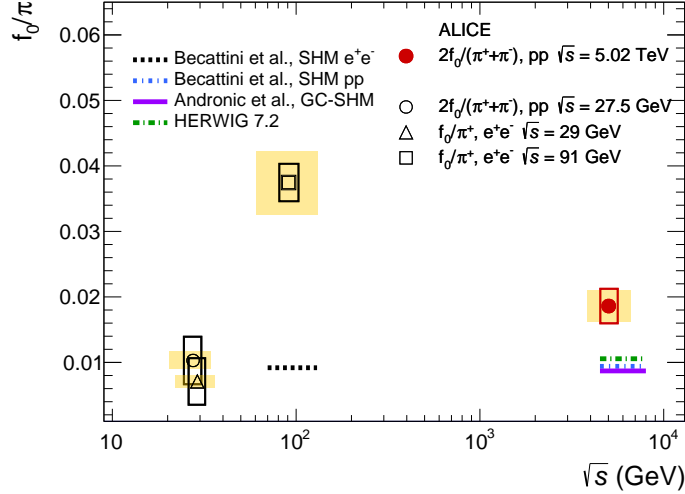


Figure 4: Comparison of the measured $2f_0/(\pi^+ + \pi^-)$ ratio with measurements in e^+e^- -collisions at $\sqrt{s} = 29$ GeV [62], $\sqrt{s} = 91$ GeV [63] and in pp collisions at $\sqrt{s} = 27.5$ GeV [64]. The ratios are compared to predictions from statistical hadronisation model (SHM) calculations for e^+e^- -collisions [65] and pp collisions [66], GC-SHM [67] and HERWIG 7.2 [49, 50]. The hollow boxes represent the total uncertainty on data. The relative uncertainty of 13% due to the branching ratio correction [42] applies to all data points and is shown as a yellow box. All error boxes are drawn with an arbitrary horizontal width for visibility.

strangeness over the correlation volume. The model considered here, with a temperature $T_{ch} = 155$ MeV and a correlation volume that spans three units of rapidity, is able to reproduce the multiplicity dependence of hadron-to-pion ratios of several species over the charged particle multiplicity range covered by the ALICE measurements at the LHC, both qualitatively and quantitatively in most cases (see Fig. 5 of [68]). In addition, to describe the multiplicity dependence of the ϕ/π ratio observed at the LHC, the model, henceforth labelled as γ_s -CSM, incorporates the incomplete equilibration of strangeness by introducing a strangeness saturation factor $\gamma_s \leq 1$. Notably, in the strangeness nonequilibrium picture a $s\bar{s}$ pair like the ϕ meson is effectively a double-strange particle ($|S| = 2$), and ALICE ϕ data seem to be best described with $|S| = 1-2$ [69]. The $f_0(980)/\pi^+$ ratio is calculated for two scenarios, first assuming that the total strangeness content of $f_0(980)$ is equal to zero (yellow continuous line) and second, assuming a total strangeness content equal to two (blue dashed line). At high multiplicity, where the strangeness content of the system saturates in presence of a QGP, the calculations for the two scenarios converge and reach the grand canonical limit.

In the first scenario ($|S| = 0$), γ_s -CSM predicts higher values for the $f_0(980)$ to pion yield ratio as compared to the second scenario ($|S| = 2$) in the low $\langle dN_{ch}/d\eta \rangle$ region. The two predictions match each other for $\langle dN_{ch}/d\eta \rangle \geq 100$. The measured $2f_0/(\pi^+ + \pi^-)$ ratio in pp collisions at $\sqrt{s} = 5.02$ TeV differs by 1.9σ from the γ_s -CSM prediction for the $f_0(980)$ with net strangeness equal to zero, and by 4.0σ from the $|S| = 2$ prediction, indicating that the former scenario is favoured over the latter in this implementation of the model.

5 Conclusions

In conclusion, the first measurement of $f_0(980)$ production in inelastic pp collisions at $\sqrt{s} = 5.02$ TeV at the LHC is presented. The measurement is performed in a wide p_T interval from 0 to 16 GeV/ c at midrapidity by reconstructing the resonance in the hadronic decay channel $f_0(980) \rightarrow \pi^+\pi^-$. The inclusive $f_0(980)$ production is underestimated by HERWIG 7.2 by a factor of two for $1 < p_T < 4$ GeV/ c and by a large factor (up to more than four) in $4 < p_T < 16$ GeV/ c . However, this QCD-inspired event

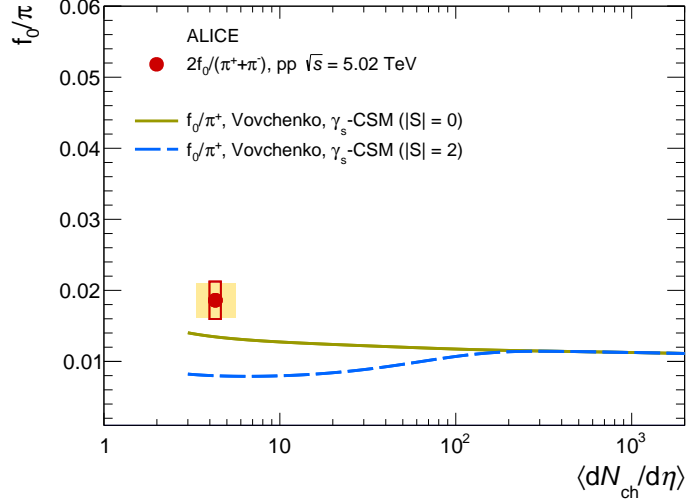


Figure 5: The $2f_0/(\pi^+ + \pi^-)$ ratio measured in pp collisions at $\sqrt{s} = 5.02$ TeV [61] is compared to two distinct predictions for f_0/π^+ from a canonical statistical model (γ_s -CSM [68], see text for details) as a function of $\langle dN_{ch}/d\eta \rangle$. The two calculations differ by the assumed strangeness content of $f_0(980)$ and correspond to zero total strangeness, $|S| = 0$ and $|S| = 2$. The height of the hollow red box represents the total uncertainty on the ratio, its width represents the uncertainty on the $\langle dN_{ch}/d\eta \rangle$. The relative uncertainty of 13% due to the branching ratio correction [42] is shown as a yellow box with an arbitrary horizontal width for visibility.

generator is able to describe the p_T -dependence of the $2f_0(980)/(\pi^+ + \pi^-)$ and $f_0(980)/\phi$ ratios in a rather broad p_T range, while failing to reproduce the $2f_0(980)/(p+\bar{p})$ ratio over the entire measured p_T range. The production of $f_0(980)$ is also not described by a AMPT+coalescence model prediction in three configurations ($s\bar{s}$ meson, $u\bar{u}s\bar{s}$ tetraquark state, and K^+K^- molecule), which use the phase space information of quarks and kaons from the AMPT model. In order to compare the new measurement of the p_T -integrated $f_0(980)$ to pion ratio with low energy data, the low energy points were updated with the latest branching ratio. The new result presented in this letter suggests a mild increase of the production of $f_0(980)$ relative to pions in inelastic pp collisions from $\sqrt{s} = 27.5$ GeV to $\sqrt{s} = 5.02$ TeV. For the same ratio, HERWIG 7.2 predicts a value that is about 43% lower than the measured one whereas different implementations of the statistical hadronisation model underestimate the data by up to a factor of about two. Notably, the γ_s -CSM prediction for the $f_0(980)$ assuming net strangeness equal to zero is consistent with the data within 1.9σ .

In summary, the description of the inclusive f_0 production in pp collisions provided by the few event generators and theoretical calculations that attempt its modelling is, at present, unsatisfactory. Future developments in this direction may help gaining insight over the nature of this particle, as new data may become available. From the experimental point of view, the results presented in this letter set the necessary baseline for the future measurements of the production and the nuclear modification factor of $f_0(980)$ in p-Pb and Pb-Pb collisions at the LHC, which have been suggested as observables that are sensitive to the elusive nature of this particle.

Acknowledgements

The ALICE Collaboration would like to thank all its engineers and technicians for their invaluable contributions to the construction of the experiment and the CERN accelerator teams for the outstanding performance of the LHC complex. The ALICE Collaboration gratefully acknowledges the resources and support provided by all Grid centres and the Worldwide LHC Computing Grid (WLCG) collaboration. The ALICE Collaboration acknowledges the following funding agencies for their support in building

and running the ALICE detector: A. I. Alikhanyan National Science Laboratory (Yerevan Physics Institute) Foundation (ANSL), State Committee of Science and World Federation of Scientists (WFS), Armenia; Austrian Academy of Sciences, Austrian Science Fund (FWF): [M 2467-N36] and Nationalstiftung für Forschung, Technologie und Entwicklung, Austria; Ministry of Communications and High Technologies, National Nuclear Research Center, Azerbaijan; Conselho Nacional de Desenvolvimento Científico e Tecnológico (CNPq), Financiadora de Estudos e Projetos (Finep), Fundação de Amparo à Pesquisa do Estado de São Paulo (FAPESP) and Universidade Federal do Rio Grande do Sul (UFRGS), Brazil; Bulgarian Ministry of Education and Science, within the National Roadmap for Research Infrastructures 2020-2027 (object CERN), Bulgaria; Ministry of Education of China (MOEC) , Ministry of Science & Technology of China (MSTC) and National Natural Science Foundation of China (NSFC), China; Ministry of Science and Education and Croatian Science Foundation, Croatia; Centro de Aplicaciones Tecnológicas y Desarrollo Nuclear (CEADEN), Cubaenergía, Cuba; Ministry of Education, Youth and Sports of the Czech Republic, Czech Republic; The Danish Council for Independent Research | Natural Sciences, the VILLUM FONDEN and Danish National Research Foundation (DNRF), Denmark; Helsinki Institute of Physics (HIP), Finland; Commissariat à l'Energie Atomique (CEA) and Institut National de Physique Nucléaire et de Physique des Particules (IN2P3) and Centre National de la Recherche Scientifique (CNRS), France; Bundesministerium für Bildung und Forschung (BMBF) and GSI Helmholtzzentrum für Schwerionenforschung GmbH, Germany; General Secretariat for Research and Technology, Ministry of Education, Research and Religions, Greece; National Research, Development and Innovation Office, Hungary; Department of Atomic Energy Government of India (DAE), Department of Science and Technology, Government of India (DST), University Grants Commission, Government of India (UGC) and Council of Scientific and Industrial Research (CSIR), India; National Research and Innovation Agency - BRIN, Indonesia; Istituto Nazionale di Fisica Nucleare (INFN), Italy; Japanese Ministry of Education, Culture, Sports, Science and Technology (MEXT) and Japan Society for the Promotion of Science (JSPS) KAKENHI, Japan; Consejo Nacional de Ciencia (CONACYT) y Tecnología, through Fondo de Cooperación Internacional en Ciencia y Tecnología (FONCICYT) and Dirección General de Asuntos del Personal Académico (DGAPA), Mexico; Nederlandse Organisatie voor Wetenschappelijk Onderzoek (NWO), Netherlands; The Research Council of Norway, Norway; Commission on Science and Technology for Sustainable Development in the South (COMSATS), Pakistan; Pontificia Universidad Católica del Perú, Peru; Ministry of Education and Science, National Science Centre and WUT ID-UB, Poland; Korea Institute of Science and Technology Information and National Research Foundation of Korea (NRF), Republic of Korea; Ministry of Education and Scientific Research, Institute of Atomic Physics, Ministry of Research and Innovation and Institute of Atomic Physics and University Politehnica of Bucharest, Romania; Ministry of Education, Science, Research and Sport of the Slovak Republic, Slovakia; National Research Foundation of South Africa, South Africa; Swedish Research Council (VR) and Knut & Alice Wallenberg Foundation (KAW), Sweden; European Organization for Nuclear Research, Switzerland; Suranaree University of Technology (SUT), National Science and Technology Development Agency (NSTDA) and National Science, Research and Innovation Fund (NSRF via PMU-B B05F650021), Thailand; Turkish Energy, Nuclear and Mineral Research Agency (TENMAK), Turkey; National Academy of Sciences of Ukraine, Ukraine; Science and Technology Facilities Council (STFC), United Kingdom; National Science Foundation of the United States of America (NSF) and United States Department of Energy, Office of Nuclear Physics (DOE NP), United States of America. In addition, individual groups or members have received support from: Marie Skłodowska Curie, European Research Council, Strong 2020 - Horizon 2020 (grant nos. 950692, 824093, 896850), European Union; Academy of Finland (Center of Excellence in Quark Matter) (grant nos. 346327, 346328), Finland; Programa de Apoyos para la Superación del Personal Académico, UNAM, Mexico.

References

- [1] M. Gell-Mann, “A Schematic Model of Baryons and Mesons”, *Phys. Lett.* **8** (1964) 214–215.

- [2] **Particle Data Group** Collaboration, P. Zyla *et al.*, “Review of Particle Physics”, *PTEP* **2020** (2020) 083C01.
- [3] R. L. Jaffe, “Multi-Quark Hadrons. 1. The Phenomenology of (2 Quark 2 anti-Quark) Mesons”, *Phys. Rev. D* **15** (1977) 267.
- [4] R. L. Jaffe, “Multi-Quark Hadrons. 2. Methods”, *Phys. Rev. D* **15** (1977) 281.
- [5] F. E. Close and N. A. Tornqvist, “Scalar mesons above and below 1-GeV”, *J. Phys. G* **28** (2002) R249–R267, arXiv:hep-ph/0204205.
- [6] C. Amsler and N. A. Tornqvist, “Mesons beyond the naive quark model”, *Phys. Rept.* **389** (2004) 61–117.
- [7] L. Maiani, F. Piccinini, A. D. Polosa, and V. Riquer, “A New look at scalar mesons”, *Phys. Rev. Lett.* **93** (2004) 212002, arXiv:hep-ph/0407017.
- [8] E. Klempt and A. Zaitsev, “Glueballs, Hybrids, Multiquarks. Experimental facts versus QCD inspired concepts”, *Phys. Rept.* **454** (2007) 1–202, arXiv:0708.4016 [hep-ph].
- [9] C.-H. Chen, “Evidence for two quark content of f(0)(980) in exclusive b → c decays”, *Phys. Rev. D* **67** (2003) 094011, arXiv:hep-ph/0302059.
- [10] N. N. Achasov, J. V. Bennett, A. V. Kiselev, E. A. Kozyrev, and G. N. Shestakov, “Evidence of the four-quark nature of $f_0(980)$ and $f_0(500)$ ”, *Phys. Rev. D* **103** (2021) 014010, arXiv:2009.04191 [hep-ph].
- [11] H. A. Ahmed and C. W. Xiao, “Study the molecular nature of σ , $f_0(980)$, and $a_0(980)$ states”, *Phys. Rev. D* **101** (2020) 094034, arXiv:2001.08141 [hep-ph].
- [12] D. Oliinychenko and C. Shen, “Resonance production in PbPb collisions at 5.02 TeV via hydrodynamics and hadronic afterburner”, arXiv:2105.07539 [hep-ph].
- [13] N. N. Achasov, “Radiative decays of phi meson about nature of light scalar resonances”, *Nucl. Phys. A* **728** (2003) 425–438, arXiv:hep-ph/0309118.
- [14] M. N. Achasov *et al.*, “The phi → eta pi0 gamma decay”, *Phys. Lett. B* **479** (2000) 53–58, arXiv:hep-ex/0003031.
- [15] **CMD-2** Collaboration, R. R. Akhmetshin *et al.*, “First observation of the phi → pi+ pi- gamma decay”, *Phys. Lett. B* **462** (1999) 371, arXiv:hep-ex/9907005.
- [16] **KLOE** Collaboration, A. Aloisio *et al.*, “Study of the decay $\phi \rightarrow \eta\pi^0\gamma$ with the KLOE detector”, *Phys. Lett. B* **536** (2002) 209–216, arXiv:hep-ex/0204012.
- [17] **KLOE** Collaboration, F. Ambrosino *et al.*, “Dalitz plot analysis of $e^+e^- \rightarrow \pi^0\pi^0\gamma$ events at \sqrt{s} approximately M(ϕ) with the KLOE detector”, *Eur. Phys. J. C* **49** (2007) 473–488, arXiv:hep-ex/0609009.
- [18] **BESIII** Collaboration, M. Ablikim *et al.*, “Amplitude analysis of the $\pi^0\pi^0$ system produced in radiative J/ ψ decays”, *Phys. Rev. D* **92** (2015) 052003, arXiv:1506.00546 [hep-ex]. [Erratum: Phys.Rev.D 93, 039906 (2016)].
- [19] **E791** Collaboration, E. M. Aitala *et al.*, “Study of the $D_s^+ \rightarrow \pi^-\pi^+\pi^+$ decay and measurement of f(0) masses and widths”, *Phys. Rev. Lett.* **86** (2001) 765–769, arXiv:hep-ex/0007027.

- [20] **LHCb** Collaboration, R. Aaij *et al.*, “Measurement of resonant and CP components in $\bar{B}_s^0 \rightarrow J/\psi \pi^+ \pi^-$ decays”, *Phys. Rev. D* **89** (2014) 092006, arXiv:1402.6248 [hep-ex].
- [21] **LHCb** Collaboration, R. Aaij *et al.*, “Measurement of the resonant and CP components in $\bar{B}^0 \rightarrow J/\psi \pi^+ \pi^-$ decays”, *Phys. Rev. D* **90** (2014) 012003, arXiv:1404.5673 [hep-ex].
- [22] J. T. Daub, C. Hanhart, and B. Kubis, “A model-independent analysis of final-state interactions in $\bar{B}_{d/s}^0 \rightarrow J/\psi \pi\pi$ ”, *JHEP* **02** (2016) 009, arXiv:1508.06841 [hep-ph].
- [23] G. Janssen, B. C. Pearce, K. Holinde, and J. Speth, “On the structure of the scalar mesons f0 (975) and a0 (980)”, *Phys. Rev. D* **52** (1995) 2690–2700, arXiv:nucl-th/9411021.
- [24] J. D. Weinstein and N. Isgur, “K anti-K Molecules”, *Phys. Rev. D* **41** (1990) 2236.
- [25] C. W. Xiao, U. G. Meißner, and J. A. Oller, “Investigation of $J/\psi \rightarrow \gamma \pi^0 \eta(\pi^+ \pi^-, \pi^0 \pi^0)$ radiative decays including final-state interactions”, *Eur. Phys. J. A* **56** (2020) 23, arXiv:1907.09072 [hep-ph].
- [26] L. Maiani, A. D. Polosa, V. Riquer, and C. A. Salgado, “Counting valence quarks at RHIC and LHC”, *Phys. Lett. B* **645** (2007) 138–145, arXiv:hep-ph/0606217.
- [27] **ExHIC** Collaboration, S. Cho *et al.*, “Exotic hadrons from heavy ion collisions”, *Prog. Part. Nucl. Phys.* **95** (2017) 279–322, arXiv:1702.00486 [nucl-th].
- [28] A. Gu, T. Edmonds, J. Zhao, and F. Wang, “Elliptical flow coalescence to identify the $f_0(980)$ content”, *Phys. Rev. C* **101** (2020) 024908, arXiv:1902.07152 [nucl-ex].
- [29] **HotQCD** Collaboration, A. Bazavov *et al.*, “Chiral crossover in QCD at zero and non-zero chemical potentials”, *Phys. Lett. B* **795** (2019) 15–21, arXiv:1812.08235 [hep-lat].
- [30] **ALICE** Collaboration, K. Aamodt *et al.*, “Two-pion Bose-Einstein correlations in central Pb-Pb collisions at $\sqrt{s_{\text{NN}}} = 2.76$ TeV”, *Phys. Lett. B* **696** (2011) 328–337, arXiv:1012.4035 [nucl-ex].
- [31] **ALICE** Collaboration, S. Acharya *et al.*, “Production of the $\rho(770)^0$ meson in pp and Pb-Pb collisions at $\sqrt{s_{\text{NN}}} = 2.76$ TeV”, *Phys. Rev. C* **99** (2019) 064901, arXiv:1805.04365 [nucl-ex].
- [32] **ALICE** Collaboration, S. Acharya *et al.*, “Evidence of rescattering effect in Pb-Pb collisions at the LHC through production of $K^*(892)^0$ and $\phi(1020)$ mesons”, *Phys. Lett. B* **802** (2020) 135225, arXiv:1910.14419 [nucl-ex].
- [33] **ALICE** Collaboration, S. Acharya *et al.*, “Suppression of $\Lambda(1520)$ resonance production in central Pb-Pb collisions at $\sqrt{s_{\text{NN}}} = 2.76$ TeV”, *Phys. Rev. C* **99** (2019) 024905, arXiv:1805.04361 [nucl-ex].
- [34] R. J. Fries, B. Muller, C. Nonaka, and S. A. Bass, “Hadronization in heavy ion collisions: Recombination and fragmentation of partons”, *Phys. Rev. Lett.* **90** (2003) 202303, arXiv:nucl-th/0301087.
- [35] V. Minissale, F. Scardina, and V. Greco, “Hadrons from coalescence plus fragmentation in AA collisions at energies available at the BNL Relativistic Heavy Ion Collider to the CERN Large Hadron Collider”, *Phys. Rev. C* **92** (2015) 054904, arXiv:1502.06213 [nucl-th].

- [36] S. Plumari, V. Minissale, S. K. Das, G. Coci, and V. Greco, “Charmed Hadrons from Coalescence plus Fragmentation in relativistic nucleus-nucleus collisions at RHIC and LHC”, *Eur. Phys. J. C* **78** (2018) 348, arXiv:1712.00730 [hep-ph].
- [37] ALICE Collaboration, B. B. Abelev *et al.*, “Performance of the ALICE Experiment at the CERN LHC”, *Int. J. Mod. Phys. A* **29** (2014) 1430044, arXiv:1402.4476 [nucl-ex].
- [38] ALICE Collaboration, K. Aamodt *et al.*, “The ALICE experiment at the CERN LHC”, *JINST* **3** (2008) S08002.
- [39] ALICE Collaboration, E. Abbas *et al.*, “Performance of the ALICE VZERO system”, *JINST* **8** (2013) P10016, arXiv:1306.3130 [nucl-ex].
- [40] STAR Collaboration, C. Adler *et al.*, “Coherent ρ^0 production in ultraperipheral heavy ion collisions”, *Phys. Rev. Lett.* **89** (2002) 272302, arXiv:nucl-ex/0206004.
- [41] ALICE Collaboration, J. Adam *et al.*, “Coherent ρ^0 photoproduction in ultra-peripheral Pb-Pb collisions at $\sqrt{s_{NN}} = 2.76$ TeV”, *JHEP* **09** (2015) 095, arXiv:1503.09177 [nucl-ex].
- [42] S. Stone and L. Zhang, “Use of $B \rightarrow J/\psi f_0$ decays to discern the $q\bar{q}$ or tetraquark nature of scalar mesons”, *Phys. Rev. Lett.* **111** (2013) 062001.
- [43] ALICE Collaboration, B. B. Abelev *et al.*, “ALICE luminosity determination for pp collisions at $\sqrt{s} = 5$ TeV”, *ALICE-PUBLIC-2016-005* (2016).
- [44] C. Loizides, J. Kamin, and D. d’Enterria, “Improved Monte Carlo Glauber predictions at present and future nuclear colliders”, *Phys. Rev.* **C97** (2018) 054910, arXiv:1710.07098 [nucl-ex]. [Erratum: *Phys. Rev.* C99,no.1,019901(2019)].
- [45] P. Skands, S. Carrazza, and J. Rojo, “Tuning PYTHIA 8.1: the Monash 2013 Tune”, *Eur. Phys. J. C* **74** (2014) 3024, arXiv:1404.5630 [hep-ph].
- [46] R. Brun, F. Bruyant, F. Carminati, S. Giani, M. Maire, A. McPherson, G. Patrick, and L. Urban, “GEANT Detector Description and Simulation Tool”, *CERN-W-5013* (10, 1994).
- [47] ALICE Collaboration, S. Acharya *et al.*, “Transverse momentum spectra and nuclear modification factors of charged particles in pp, p-Pb and Pb-Pb collisions at the LHC”, *JHEP* **11** (2018) 013, arXiv:1802.09145 [nucl-ex].
- [48] ALICE Collaboration, J. Adam *et al.*, “Measurement of pion, kaon and proton production in proton–proton collisions at $\sqrt{s} = 7$ TeV”, *Eur. Phys. J. C* **75** (2015) 226, arXiv:1504.00024 [nucl-ex].
- [49] J. Bellm *et al.*, “Herwig 7.0/Herwig++ 3.0 release note”, *Eur. Phys. J. C* **76** (2016) 196, arXiv:1512.01178 [hep-ph].
- [50] M. Bahr *et al.*, “Herwig++ Physics and Manual”, *Eur. Phys. J. C* **58** (2008) 639–707, arXiv:0803.0883 [hep-ph].
- [51] Z.-W. Lin, C. M. Ko, B.-A. Li, B. Zhang, and S. Pal, “A Multi-phase transport model for relativistic heavy ion collisions”, *Phys. Rev. C* **72** (2005) 064901, arXiv:nucl-th/0411110.
- [52] B.-A. Li and C. M. Ko, “Formation of superdense hadronic matter in high-energy heavy ion collisions”, *Phys. Rev. C* **52** (1995) 2037–2063, arXiv:nucl-th/9505016.
- [53] B. Li, A. T. Sustich, B. Zhang, and C. M. Ko, “Studies of superdense hadronic matter in a relativistic transport model”, *Int. J. Mod. Phys. E* **10** (2001) 267–352.

- [54] X.-N. Wang and M. Gyulassy, “HIJING: A Monte Carlo model for multiple jet production in p p, p A and A A collisions”, *Phys. Rev. D* **44** (1991) 3501–3516.
- [55] B. Zhang, “ZPC 1.0.1: A Parton cascade for ultrarelativistic heavy ion collisions”, *Comput. Phys. Commun.* **109** (1998) 193–206, arXiv:nucl-th/9709009.
- [56] B. Andersson, G. Gustafson, and B. Soderberg, “A General Model for Jet Fragmentation”, *Z. Phys. C* **20** (1983) 317.
- [57] B. Andersson, G. Gustafson, G. Ingelman, and T. Sjöstrand, “Parton Fragmentation and String Dynamics”, *Phys. Rept.* **97** (1983) 31–145.
- [58] T. Sjöstrand, “High-energy physics event generation with PYTHIA 5.7 and JETSET 7.4”, *Comput. Phys. Commun.* **82** (1994) 74–90.
- [59] Z.-w. Lin and C. M. Ko, “Partonic effects on the elliptic flow at RHIC”, *Phys. Rev. C* **65** (2002) 034904, arXiv:nucl-th/0108039.
- [60] P. Lebiedowicz, R. Maciąła, and A. Szczurek, “Production of $f_0(980)$ meson at the LHC: Color evaporation versus color-singlet gluon-gluon fusion”, *Phys. Lett. B* **806** (2020) 135475, arXiv:2003.08200 [hep-ph].
- [61] **ALICE** Collaboration, S. Acharya *et al.*, “Production of charged pions, kaons, and (anti-)protons in Pb–Pb and inelastic pp collisions at $\sqrt{s_{\text{NN}}} = 5.02$ TeV”, *Phys. Rev. C* **101** (2020) 044907, arXiv:1910.07678 [nucl-ex].
- [62] W. Hofmann, “Particle Composition in Hadronic Jets in e^+e^- Annihilation”, *Ann. Rev. Nucl. Part. Sci.* **38** (1988) 279–322.
- [63] P. V. Chliapnikov, “Hyperfine Splitting in Light-Flavour Hadron Production at LEP”, *Phys. Lett. B* **462** (1999) 341–353.
- [64] M. Aguilar-Benitez *et al.*, “Inclusive particle production in 400-GeV/c pp interactions”, *Z. Phys. C* **50** (1991) 405–426.
- [65] F. Becattini, P. Castorina, J. Manninen, and H. Satz, “The Thermal Production of Strange and Non-Strange Hadrons in e^+e^- Collisions”, *Eur. Phys. J. C* **56** (2008) 493–510, arXiv:0805.0964 [hep-ph].
- [66] F. Becattini and U. W. Heinz, “Thermal hadron production in p p and p anti-p collisions”, *Z. Phys. C* **76** (1997) 269–286, arXiv:hep-ph/9702274. [Erratum: Z.Phys.C 76, 578 (1997)].
- [67] A. Andronic, P. Braun-Munzinger, K. Redlich, and J. Stachel, “Decoding the phase structure of QCD via particle production at high energy”, *Nature* **561** (2018) 321–330, arXiv:1710.09425 [nucl-th].
- [68] V. Vovchenko, B. Dönigus, and H. Stoecker, “Canonical statistical model analysis of p-p , p -Pb, and Pb-Pb collisions at energies available at the CERN Large Hadron Collider”, *Phys. Rev. C* **100** (2019) 054906, arXiv:1906.03145 [hep-ph].
- [69] **ALICE** Collaboration, B. B. Abelev *et al.*, “ $K^*(892)^0$ and $\phi(1020)$ production in Pb-Pb collisions at $\sqrt{s_{\text{NN}}} = 2.76$ TeV”, *Phys. Rev. C* **91** (2015) 024609, arXiv:1404.0495 [nucl-ex].

A The ALICE Collaboration

- S. Acharya ¹²⁴, D. Adamová ⁸⁵, A. Adler⁶⁹, G. Aglieri Rinella ³², M. Agnello ²⁹, N. Agrawal ⁵⁰, Z. Ahammed ¹³², S. Ahmad ¹⁵, S.U. Ahn ⁷⁰, I. Ahuja ³⁷, A. Akindinov ¹⁴⁰, M. Al-Turany ⁹⁷, D. Aleksandrov ¹⁴⁰, B. Alessandro ⁵⁵, H.M. Alfanda ⁶, R. Alfaro Molina ⁶⁶, B. Ali ¹⁵, Y. Ali ¹³, A. Alici ²⁵, N. Alizadehvandchali ¹¹³, A. Alkin ³², J. Alme ²⁰, G. Alocco ⁵¹, T. Alt ⁶³, I. Altsybeev ¹⁴⁰, M.N. Anaam ⁶, C. Andrei ⁴⁵, A. Andronic ¹³⁵, V. Anguelov ⁹⁴, F. Antinori ⁵³, P. Antonioli ⁵⁰, C. Anuj ¹⁵, N. Apadula ⁷³, L. Aphecetche ¹⁰³, H. Appelshäuser ⁶³, C. Arata ⁷², S. Arcelli ²⁵, M. Aresti ⁵¹, R. Arnaldi ⁵⁵, I.C. Arsene ¹⁹, M. Arslanbekov ¹³⁷, A. Augustinus ³², R. Averbeck ⁹⁷, S. Aziz ¹²⁸, M.D. Azmi ¹⁵, A. Badalà ⁵², Y.W. Baek ⁴⁰, X. Bai ¹¹⁷, R. Bailhache ⁶³, Y. Bailung ⁴⁷, R. Bala ⁹⁰, A. Balbino ²⁹, A. Baldissari ¹²⁷, B. Balis ², D. Banerjee ⁴, Z. Banoo ⁹⁰, R. Barbera ²⁶, L. Barioglio ⁹⁵, M. Barlou ⁷⁷, G.G. Barnaföldi ¹³⁶, L.S. Barnby ⁸⁴, V. Barret ¹²⁴, L. Barreto ¹⁰⁹, C. Bartels ¹¹⁶, K. Barth ³², E. Bartsch ⁶³, F. Baruffaldi ²⁷, N. Bastid ¹²⁴, S. Basu ⁷⁴, G. Batigne ¹⁰³, D. Battistini ⁹⁵, B. Batyunya ¹⁴¹, D. Bauri ⁴⁶, J.L. Bazo Alba ¹⁰¹, I.G. Bearden ⁸², C. Beattie ¹³⁷, P. Becht ⁹⁷, D. Behera ⁴⁷, I. Belikov ¹²⁶, A.D.C. Bell Hechavarria ¹³⁵, F. Bellini ²⁵, R. Bellwied ¹¹³, S. Belokurova ¹⁴⁰, V. Belyaev ¹⁴⁰, G. Bencedi ^{136,64}, S. Beole ²⁴, A. Bercuci ⁴⁵, Y. Berdnikov ¹⁴⁰, A. Berdnikova ⁹⁴, L. Bergmann ⁹⁴, M.G. Besouï ⁶², L. Betev ³², P.P. Bhaduri ¹³², A. Bhasin ⁹⁰, M.A. Bhat ⁴, B. Bhattacharjee ⁴¹, L. Bianchi ²⁴, N. Bianchi ⁴⁸, J. Bielčík ³⁵, J. Bielčíková ⁸⁵, J. Biernat ¹⁰⁶, A.P. Bigot ¹²⁶, A. Bilandzic ⁹⁵, G. Biro ¹³⁶, S. Biswas ⁴, N. Bize ¹⁰³, J.T. Blair ¹⁰⁷, D. Blau ¹⁴⁰, M.B. Blidaru ⁹⁷, N. Bluhme ³⁸, C. Blume ⁶³, G. Boca ^{21,54}, F. Bock ⁸⁶, T. Bodova ²⁰, A. Bogdanov ¹⁴⁰, S. Boi ²², J. Bok ⁵⁷, L. Boldizsár ¹³⁶, A. Bolozdynya ¹⁴⁰, M. Bombara ³⁷, P.M. Bond ³², G. Bonomi ^{131,54}, H. Borel ¹²⁷, A. Borissov ¹⁴⁰, H. Bossi ¹³⁷, E. Botta ²⁴, L. Bratrud ⁶³, P. Braun-Munzinger ⁹⁷, M. Bregant ¹⁰⁹, M. Broz ³⁵, G.E. Bruno ^{96,31}, M.D. Buckland ¹¹⁶, D. Budnikov ¹⁴⁰, H. Buesching ⁶³, S. Bufalino ²⁹, O. Bugnon ¹⁰³, P. Buhler ¹⁰², Z. Buthelezi ^{67,120}, J.B. Butt ¹³, S.A. Bysiak ¹⁰⁶, M. Cai ^{27,6}, H. Caines ¹³⁷, A. Caliva ⁹⁷, E. Calvo Villar ¹⁰¹, J.M.M. Camacho ¹⁰⁸, P. Camerini ²³, F.D.M. Canedo ¹⁰⁹, M. Carabas ¹²³, F. Carnesecchi ³², R. Caron ¹²⁵, J. Castillo Castellanos ¹²⁷, F. Catalano ^{24,29}, C. Ceballos Sanchez ¹⁴¹, I. Chakaberia ⁷³, P. Chakraborty ⁴⁶, S. Chandra ¹³², S. Chapelard ³², M. Chartier ¹¹⁶, S. Chattopadhyay ¹³², S. Chattopadhyay ⁹⁹, T.G. Chavez ⁴⁴, T. Cheng ⁶, C. Cheshkov ¹²⁵, B. Cheynis ¹²⁵, V. Chibante Barroso ³², D.D. Chinellato ¹¹⁰, E.S. Chizzali ^{II,95}, J. Cho ⁵⁷, S. Cho ⁵⁷, P. Chochula ³², P. Christakoglou ⁸³, C.H. Christensen ⁸², P. Christiansen ⁷⁴, T. Chujo ¹²², M. Ciaccio ²⁹, C. Cicalo ⁵¹, L. Cifarelli ²⁵, F. Cindolo ⁵⁰, M.R. Ciupek ⁹⁷, G. Clai ^{III,50}, F. Colamaria ⁴⁹, J.S. Colburn ¹⁰⁰, D. Colella ^{96,31}, A. Collu ⁷³, M. Colocci ³², M. Concas ^{IV,55}, G. Conesa Balbastre ⁷², Z. Conesa del Valle ¹²⁸, G. Contin ²³, J.G. Contreras ³⁵, M.L. Coquet ¹²⁷, T.M. Cormier ^{I,86}, P. Cortese ^{130,55}, M.R. Cosentino ¹¹¹, F. Costa ³², S. Costanza ^{21,54}, J. Crkovská ⁹⁴, P. Crochet ¹²⁴, R. Cruz-Torres ⁷³, E. Cuautle ⁶⁴, P. Cui ⁶, L. Cunqueiro ⁸⁶, A. Dainese ⁵³, M.C. Danisch ⁹⁴, A. Danu ⁶², P. Das ⁷⁹, P. Das ⁴, S. Das ⁴, A.R. Dash ¹³⁵, S. Dash ⁴⁶, R.M.H. David ⁴⁴, A. De Caro ²⁸, G. de Cataldo ⁴⁹, L. De Cilladi ²⁴, J. de Cuveland ³⁸, A. De Falco ²², D. De Gruttola ²⁸, N. De Marco ⁵⁵, C. De Martin ²³, S. De Pasquale ²⁸, S. Deb ⁴⁷, R.J. Debski ², K.R. Deja ¹³³, R. Del Grande ⁹⁵, L. Dello Stritto ²⁸, W. Deng ⁶, P. Dhankher ¹⁸, D. Di Bari ³¹, A. Di Mauro ³², R.A. Diaz ^{141,7}, T. Dietel ¹¹², Y. Ding ^{125,6}, R. Divià ³², D.U. Dixit ¹⁸, Ø. Djupsland ²⁰, U. Dmitrieva ¹⁴⁰, A. Dobrin ⁶², B. Dönigus ⁶³, A.K. Dubey ¹³², J.M. Dubinski ¹³³, A. Dubla ⁹⁷, S. Dudi ⁸⁹, P. Dupieux ¹²⁴, M. Durkac ¹⁰⁵, N. Dzalaiova ¹², T.M. Eder ¹³⁵, R.J. Ehlers ⁸⁶, V.N. Eikeland ²⁰, F. Eisenhut ⁶³, D. Elia ⁴⁹, B. Erazmus ¹⁰³, F. Ercolelli ²⁵, F. Erhardt ⁸⁸, M.R. Ersdal ²⁰, B. Espagnon ¹²⁸, G. Eulisse ³², D. Evans ¹⁰⁰, S. Evdokimov ¹⁴⁰, L. Fabbietti ⁹⁵, M. Faggin ²⁷, J. Faivre ⁷², F. Fan ⁶, W. Fan ⁷³, A. Fantoni ⁴⁸, M. Fasel ⁸⁶, P. Fecchio ²⁹, A. Feliciello ⁵⁵, G. Feofilov ¹⁴⁰, A. Fernández Téllez ⁴⁴, M.B. Ferrer ³², A. Ferrero ¹²⁷, C. Ferrero ⁵⁵, A. Ferretti ²⁴, V.J.G. Feuillard ⁹⁴, V. Filova ³⁵, D. Finogeev ¹⁴⁰, F.M. Fionda ⁵¹, G. Fiorenza ⁹⁶, F. Flor ¹¹³, A.N. Flores ¹⁰⁷, S. Foertsch ⁶⁷, I. Fokin ⁹⁴, S. Fokin ¹⁴⁰, E. Fragiaco ⁵⁶, E. Frajna ¹³⁶, U. Fuchs ³², N. Funicello ²⁸, C. Furget ⁷², A. Furs ¹⁴⁰, T. Fusayasu ⁹⁸, J.J. Gaardhøje ⁸², M. Gagliardi ²⁴, A.M. Gago ¹⁰¹, A. Gal ¹²⁶, C.D. Galvan ¹⁰⁸, D.R. Gangadharan ¹¹³, P. Ganoti ⁷⁷, C. Garabatos ⁹⁷, J.R.A. Garcia ⁴⁴, E. Garcia-Solis ⁹, K. Garg ¹⁰³, C. Gargiulo ³², A. Garibaldi ⁸⁰, K. Garner ¹³⁵, A. Gautam ¹¹⁵, M.B. Gay Ducati ⁶⁵, M. Germain ¹⁰³, C. Ghosh ¹³², S.K. Ghosh ⁴, M. Giacalone ²⁵, P. Gianotti ⁴⁸, P. Giubellino ^{97,55}, P. Giubilato ²⁷, A.M.C. Glaenzer ¹²⁷, P. Glässel ⁹⁴, E. Glimos ¹¹⁹, D.J.Q. Goh ⁷⁵, V. Gonzalez ¹³⁴, L.H. González-Trueba ⁶⁶, M. Gorgon ², S. Gotovac ³³, V. Grabski ⁶⁶, L.K. Graczykowski ¹³³, E. Grecka ⁸⁵, L. Greiner ⁷³, A. Grelli ⁵⁸, C. Grigoras ³², V. Grigoriev ¹⁴⁰, S. Grigoryan ^{141,1}, F. Grossa ³², J.F. Grosse-Oetringhaus ³², R. Grossi ⁹⁷, D. Grund ³⁵, G.G. Guardiano ¹¹⁰,

- R. Guernane ⁷², M. Guilbaud ¹⁰³, K. Gulbrandsen ⁸², T. Gunji ¹²¹, W. Guo ⁶, A. Gupta ⁹⁰, R. Gupta ⁹⁰, S.P. Guzman ⁴⁴, L. Gyulai ¹³⁶, M.K. Habib ⁹⁷, C. Hadjidakis ¹²⁸, H. Hamagaki ⁷⁵, M. Hamid ⁶, Y. Han ¹³⁸, R. Hannigan ¹⁰⁷, M.R. Haque ¹³³, A. Harlenderova ⁹⁷, J.W. Harris ¹³⁷, A. Harton ⁹, H. Hassan ⁸⁶, D. Hatzifotiadou ⁵⁰, P. Hauer ⁴², L.B. Havener ¹³⁷, S.T. Heckel ⁹⁵, E. Hellbär ⁹⁷, H. Helstrup ³⁴, T. Herman ³⁵, G. Herrera Corral ⁸, F. Herrmann ¹³⁵, S. Herrmann ¹²⁵, K.F. Hetland ³⁴, B. Heybeck ⁶³, H. Hillemanns ³², C. Hills ¹¹⁶, B. Hippolyte ¹²⁶, B. Hofman ⁵⁸, B. Hohlweger ⁸³, J. Honermann ¹³⁵, G.H. Hong ¹³⁸, D. Horak ³⁵, A. Horzyk ², R. Hosokawa ¹⁴, Y. Hou ⁶, P. Hristov ³², C. Hughes ¹¹⁹, P. Huhn ⁶³, L.M. Huhta ¹¹⁴, C.V. Hulse ¹²⁸, T.J. Humanic ⁸⁷, H. Hushnud ⁹⁹, A. Hutson ¹¹³, D. Hutter ³⁸, J.P. Iddon ¹¹⁶, R. Ilkaev ¹⁴⁰, H. Ilyas ¹³, M. Inaba ¹²², G.M. Innocenti ³², M. Ippolitov ¹⁴⁰, A. Isakov ⁸⁵, T. Isidori ¹¹⁵, M.S. Islam ⁹⁹, M. Ivanov ⁹⁷, M. Ivanov ¹², V. Ivanov ¹⁴⁰, V. Izucheev ¹⁴⁰, M. Jablonski ², B. Jacak ⁷³, N. Jacazio ³², P.M. Jacobs ⁷³, S. Jadlovska ¹⁰⁵, J. Jadlovsky ¹⁰⁵, S. Jaelani ⁸¹, L. Jaffe ³⁸, C. Jahnke ¹¹⁰, M.A. Janik ¹³³, T. Janson ⁶⁹, M. Jercic ⁸⁸, O. Jevons ¹⁰⁰, A.A.P. Jimenez ⁶⁴, F. Jonas ⁸⁶, P.G. Jones ¹⁰⁰, J.M. Jowett ^{32,97}, J. Jung ⁶³, M. Jung ⁶³, A. Junique ³², A. Jusko ¹⁰⁰, M.J. Kabus ^{32,133}, J. Kaewjai ¹⁰⁴, P. Kalinak ⁵⁹, A.S. Kalteyer ⁹⁷, A. Kalweit ³², V. Kaplin ¹⁴⁰, A. Karasu Uysal ⁷¹, D. Karatovic ⁸⁸, O. Karavichev ¹⁴⁰, T. Karavicheva ¹⁴⁰, P. Karczmarczyk ¹³³, E. Karpechev ¹⁴⁰, V. Kashyap ⁷⁹, A. Kazantsev ¹⁴⁰, U. Kebschull ⁶⁹, R. Keidel ¹³⁹, D.L.D. Keijdener ⁵⁸, M. Keil ³², B. Ketzer ⁴², A.M. Khan ⁶, S. Khan ¹⁵, A. Khanzadeev ¹⁴⁰, Y. Kharlov ¹⁴⁰, A. Khatun ¹⁵, A. Khuntia ¹⁰⁶, B. Kileng ³⁴, B. Kim ¹⁶, C. Kim ¹⁶, D.J. Kim ¹¹⁴, E.J. Kim ⁶⁸, J. Kim ¹³⁸, J.S. Kim ⁴⁰, J. Kim ⁹⁴, J. Kim ⁶⁸, M. Kim ⁹⁴, S. Kim ¹⁷, T. Kim ¹³⁸, K. Kimura ⁹², S. Kirsch ⁶³, I. Kisel ³⁸, S. Kiselev ¹⁴⁰, A. Kisiel ¹³³, J.P. Kitowski ², J.L. Klay ⁵, J. Klein ³², S. Klein ⁷³, C. Klein-Bösing ¹³⁵, M. Kleiner ⁶³, T. Klemenz ⁹⁵, A. Kluge ³², A.G. Knospe ¹¹³, C. Kobdaj ¹⁰⁴, T. Kollegger ⁹⁷, A. Kondratyev ¹⁴¹, E. Kondratyuk ¹⁴⁰, J. Konig ⁶³, S.A. Konigstorfer ⁹⁵, P.J. Konopka ³², G. Kornakov ¹³³, S.D. Koryciak ², A. Kotliarov ⁸⁵, O. Kovalenko ⁷⁸, V. Kovalenko ¹⁴⁰, M. Kowalski ¹⁰⁶, I. Králik ⁵⁹, A. Kravčáková ³⁷, L. Kreis ⁹⁷, M. Krivda ^{100,59}, F. Krizek ⁸⁵, K. Krizkova Gajdosova ³⁵, M. Kroesen ⁹⁴, M. Krüger ⁶³, D.M. Krupova ³⁵, E. Kryshen ¹⁴⁰, M. Krzewicki ³⁸, V. Kučera ³², C. Kuhn ¹²⁶, P.G. Kuijer ⁸³, T. Kumaoka ¹²², D. Kumar ¹³², L. Kumar ⁸⁹, N. Kumar ⁸⁹, S. Kumar ³¹, S. Kundu ³², P. Kurashvili ⁷⁸, A. Kurepin ¹⁴⁰, A.B. Kurepin ¹⁴⁰, S. Kushpil ⁸⁵, J. Kvapil ¹⁰⁰, M.J. Kweon ⁵⁷, J.Y. Kwon ⁵⁷, Y. Kwon ¹³⁸, S.L. La Pointe ³⁸, P. La Rocca ²⁶, Y.S. Lai ⁷³, A. Lakrathok ¹⁰⁴, M. Lamanna ³², R. Langoy ¹¹⁸, P. Larionov ⁴⁸, E. Laudi ³², L. Lautner ^{32,95}, R. Lavicka ¹⁰², T. Lazareva ¹⁴⁰, R. Lea ^{131,54}, G. Legras ¹³⁵, J. Lehrbach ³⁸, R.C. Lemmon ⁸⁴, I. León Monzón ¹⁰⁸, M.M. Lesch ⁹⁵, E.D. Lesser ¹⁸, M. Lettrich ⁹⁵, P. Lévai ¹³⁶, X. Li ¹⁰, X.L. Li ⁶, J. Lien ¹¹⁸, R. Lietava ¹⁰⁰, B. Lim ¹⁶, S.H. Lim ¹⁶, V. Lindenstruth ³⁸, A. Lindner ⁴⁵, C. Lippmann ⁹⁷, A. Liu ¹⁸, D.H. Liu ⁶, J. Liu ¹¹⁶, I.M. Lofnes ²⁰, C. Loizides ⁸⁶, P. Loncar ³³, J.A. Lopez ⁹⁴, X. Lopez ¹²⁴, E. López Torres ⁷, P. Lu ^{97,117}, J.R. Luhder ¹³⁵, M. Lunardon ²⁷, G. Luparello ⁵⁶, Y.G. Ma ³⁹, A. Maevskaya ¹⁴⁰, M. Mager ³², T. Mahmoud ⁴², A. Maire ¹²⁶, M. Malaei ¹⁴⁰, G. Malfattore ²⁵, N.M. Malik ⁹⁰, Q.W. Malik ¹⁹, S.K. Malik ⁹⁰, L. Malinina ^{VII,141}, D. Mal'Kevich ¹⁴⁰, D. Mallick ⁷⁹, N. Mallick ⁴⁷, G. Mandaglio ^{30,52}, V. Manko ¹⁴⁰, F. Manso ¹²⁴, V. Manzari ⁴⁹, Y. Mao ⁶, G.V. Margagliotti ²³, A. Margotti ⁵⁰, A. Marín ⁹⁷, C. Markert ¹⁰⁷, M. Marquard ⁶³, P. Martinengo ³², J.L. Martinez ¹¹³, M.I. Martínez ⁴⁴, G. Martínez García ¹⁰³, S. Masciocchi ⁹⁷, M. Masera ²⁴, A. Masoni ⁵¹, L. Massacrier ¹²⁸, A. Mastroserio ^{129,49}, A.M. Mathis ⁹⁵, O. Matonoha ⁷⁴, P.F.T. Matuoka ¹⁰⁹, A. Matyja ¹⁰⁶, C. Mayer ¹⁰⁶, A.L. Mazuecos ³², F. Mazzaschi ²⁴, M. Mazzilli ³², J.E. Mdhluli ¹²⁰, A.F. Mechler ⁶³, Y. Melikyan ¹⁴⁰, A. Menchaca-Rocha ⁶⁶, E. Meninno ^{102,28}, A.S. Menon ¹¹³, M. Meres ¹², S. Mhlanga ^{112,67}, Y. Miake ¹²², L. Micheletti ⁵⁵, L.C. Migliorin ¹²⁵, D.L. Mihaylov ⁹⁵, K. Mihaylov ^{141,140}, A.N. Mishra ¹³⁶, D. Miśkowiec ⁹⁷, A. Modak ⁴, A.P. Mohanty ⁵⁸, B. Mohanty ⁷⁹, M. Mohisin Khan ^{V,15}, M.A. Molander ⁴³, Z. Moravcova ⁸², C. Mordasini ⁹⁵, D.A. Moreira De Godoy ¹³⁵, I. Morozov ¹⁴⁰, A. Morsch ³², T. Mrnjavac ³², V. Muccifora ⁴⁸, S. Muhuri ¹³², J.D. Mulligan ⁷³, A. Mulliri ²², M.G. Munhoz ¹⁰⁹, R.H. Munzer ⁶³, H. Murakami ¹²¹, S. Murray ¹¹², L. Musa ³², J. Musinsky ⁵⁹, J.W. Myrcha ¹³³, B. Naik ¹²⁰, R. Nair ⁷⁸, A.I. Nambrath ¹⁸, B.K. Nandi ⁴⁶, R. Nania ⁵⁰, E. Nappi ⁴⁹, A.F. Nassirpour ⁷⁴, A. Nath ⁹⁴, C. Nattrass ¹¹⁹, A. Neagu ¹⁹, A. Negru ¹²³, L. Nellen ⁶⁴, S.V. Nesbo ³⁴, G. Neskovic ³⁸, D. Nesterov ¹⁴⁰, B.S. Nielsen ⁸², E.G. Nielsen ⁸², S. Nikolaev ¹⁴⁰, S. Nikulin ¹⁴⁰, V. Nikulin ¹⁴⁰, F. Noferini ⁵⁰, S. Noh ¹¹, P. Nomokonov ¹⁴¹, J. Norman ¹¹⁶, N. Novitzky ¹²², P. Nowakowski ¹³³, A. Nyanin ¹⁴⁰, J. Nystrand ²⁰, M. Ogino ⁷⁵, A. Ohlson ⁷⁴, V.A. Okorokov ¹⁴⁰, J. Oleniacz ¹³³, A.C. Oliveira Da Silva ¹¹⁹, M.H. Oliver ¹³⁷, A. Onnerstad ¹¹⁴, C. Oppedisano ⁵⁵, A. Ortiz Velasquez ⁶⁴, A. Oskarsson ⁷⁴, J. Otwinowski ¹⁰⁶, M. Oya ⁹², K. Oyama ⁷⁵, Y. Pachmayer ⁹⁴, S. Padhan ⁴⁶, D. Pagano ^{131,54},

- G. Paić ⁶⁴, A. Palasciano ⁴⁹, S. Panebianco ¹²⁷, H. Park ¹²², J. Park ⁵⁷, J.E. Parkkila ^{32,114}, S.P. Pathak ¹¹³, R.N. Patra ⁹⁰, B. Paul ²², H. Pei ⁶, T. Peitzmann ⁵⁸, X. Peng ⁶, M. Pennisi ²⁴, L.G. Pereira ⁶⁵, H. Pereira Da Costa ¹²⁷, D. Peresunko ¹⁴⁰, G.M. Perez ⁷, S. Perrin ¹²⁷, Y. Pestov ¹⁴⁰, V. Petráček ³⁵, V. Petrov ¹⁴⁰, M. Petrovici ⁴⁵, R.P. Pezzi ^{103,65}, S. Piano ⁵⁶, M. Pikna ¹², P. Pillot ¹⁰³, O. Pinazza ^{50,32}, L. Pinsky ¹¹³, C. Pinto ⁹⁵, S. Pisano ⁴⁸, M. Płoskoń ⁷³, M. Planinic ⁸⁸, F. Pliquet ⁶³, M.G. Poghosyan ⁸⁶, S. Politano ²⁹, N. Poljak ⁸⁸, A. Pop ⁴⁵, S. Porteboeuf-Houssais ¹²⁴, J. Porter ⁷³, V. Pozdniakov ¹⁴¹, S.K. Prasad ⁴, S. Prasad ⁴⁷, R. Preghenella ⁵⁰, F. Prino ⁵⁵, C.A. Pruneau ¹³⁴, I. Pshenichnov ¹⁴⁰, M. Puccio ³², S. Pucillo ²⁴, Z. Pugelova ¹⁰⁵, S. Qiu ⁸³, L. Quaglia ²⁴, R.E. Quishpe ¹¹³, S. Ragoni ^{14,100}, A. Rakotozafindrabe ¹²⁷, L. Ramello ^{130,55}, F. Rami ¹²⁶, S.A.R. Ramirez ⁴⁴, T.A. Rancien ⁷², R. Raniwala ⁹¹, S. Raniwala ⁹¹, S.S. Räsänen ⁴³, R. Rath ^{50,47}, I. Ravasenga ⁸³, K.F. Read ^{86,119}, A.R. Redelbach ³⁸, K. Redlich ^{VI,78}, A. Rehman ²⁰, P. Reichelt ⁶³, F. Reidt ³², H.A. Reme-Ness ³⁴, Z. Rescakova ³⁷, K. Reygers ⁹⁴, A. Riabov ¹⁴⁰, V. Riabov ¹⁴⁰, R. Ricci ²⁸, T. Richert ⁷⁴, M. Richter ¹⁹, A.A. Riedel ⁹⁵, W. Riegler ³², F. Riggi ²⁶, C. Ristea ⁶², M. Rodríguez Cahuantzi ⁴⁴, K. Røed ¹⁹, R. Rogalev ¹⁴⁰, E. Rogochaya ¹⁴¹, T.S. Rogoschinski ⁶³, D. Rohr ³², D. Röhrich ²⁰, P.F. Rojas ⁴⁴, S. Rojas Torres ³⁵, P.S. Rokita ¹³³, G. Romanenko ¹⁴¹, F. Ronchetti ⁴⁸, A. Rosano ^{30,52}, E.D. Rosas ⁶⁴, A. Rossi ⁵³, A. Roy ⁴⁷, P. Roy ⁹⁹, S. Roy ⁴⁶, N. Rubini ²⁵, D. Ruggiano ¹³³, R. Rui ²³, B. Rumyantsev ¹⁴¹, P.G. Russek ², R. Russo ⁸³, A. Rustamov ⁸⁰, E. Ryabinkin ¹⁴⁰, Y. Ryabov ¹⁴⁰, A. Rybicki ¹⁰⁶, H. Rytkonen ¹¹⁴, W. Rzesz ¹³³, O.A.M. Saarimaki ⁴³, R. Sadek ¹⁰³, S. Sadhu ³¹, S. Sadovsky ¹⁴⁰, J. Saetre ²⁰, K. Šafařík ³⁵, S. Saha ⁷⁹, B. Sahoo ⁴⁶, R. Sahoo ⁴⁷, S. Sahoo ⁶⁰, D. Sahu ⁴⁷, P.K. Sahu ⁶⁰, J. Saini ¹³², K. Sajdakova ³⁷, S. Sakai ¹²², M.P. Salvan ⁹⁷, S. Sambyal ⁹⁰, T.B. Saramela ¹⁰⁹, D. Sarkar ¹³⁴, N. Sarkar ¹³², P. Sarma ⁴¹, V. Sarritzu ²², V.M. Sarti ⁹⁵, M.H.P. Sas ¹³⁷, J. Schambach ⁸⁶, H.S. Scheid ⁶³, C. Schiaua ⁴⁵, R. Schicker ⁹⁴, A. Schmah ⁹⁴, C. Schmidt ⁹⁷, H.R. Schmidt ⁹³, M.O. Schmidt ³², M. Schmidt ⁹³, N.V. Schmidt ⁸⁶, A.R. Schmier ¹¹⁹, R. Schotter ¹²⁶, J. Schukraft ³², K. Schwarz ⁹⁷, K. Schweda ⁹⁷, G. Scioli ²⁵, E. Scomparin ⁵⁵, J.E. Seger ¹⁴, Y. Sekiguchi ¹²¹, D. Sekihata ¹²¹, I. Selyuzhenkov ^{97,140}, S. Senyukov ¹²⁶, J.J. Seo ⁵⁷, D. Serebryakov ¹⁴⁰, L. Šerkšnytė ⁹⁵, A. Sevcenco ⁶², T.J. Shaba ⁶⁷, A. Shabetai ¹⁰³, R. Shahoyan ³², A. Shangaraev ¹⁴⁰, A. Sharma ⁸⁹, D. Sharma ⁴⁶, H. Sharma ¹⁰⁶, M. Sharma ⁹⁰, N. Sharma ⁸⁹, S. Sharma ⁷⁵, S. Sharma ⁹⁰, U. Sharma ⁹⁰, A. Shatat ¹²⁸, O. Sheibani ¹¹³, K. Shigaki ⁹², M. Shimomura ⁷⁶, S. Shirinkin ¹⁴⁰, Q. Shou ³⁹, Y. Sibirski ¹⁴⁰, S. Siddhanta ⁵¹, T. Siemiaczuk ⁷⁸, T.F. Silva ¹⁰⁹, D. Silvermyr ⁷⁴, T. Simantathammakul ¹⁰⁴, R. Simeonov ³⁶, B. Singh ⁹⁰, B. Singh ⁹⁵, R. Singh ⁷⁹, R. Singh ⁹⁰, R. Singh ⁴⁷, S. Singh ¹⁵, V.K. Singh ¹³², V. Singhal ¹³², T. Sinha ⁹⁹, B. Sitar ¹², M. Sitta ^{130,55}, T.B. Skaali ¹⁹, G. Skorodumovs ⁹⁴, M. Slupecki ⁴³, N. Smirnov ¹³⁷, R.J.M. Snellings ⁵⁸, E.H. Solheim ¹⁹, C. Soncco ¹⁰¹, J. Song ¹¹³, A. Songmoolnak ¹⁰⁴, F. Soramel ²⁷, S.P. Sorensen ¹¹⁹, R. Spijkers ⁸³, I. Sputowska ¹⁰⁶, J. Staa ⁷⁴, J. Stachel ⁹⁴, I. Stan ⁶², P.J. Steffanic ¹¹⁹, S.F. Stiefelmaier ⁹⁴, D. Stocco ¹⁰³, I. Storehaug ¹⁹, M.M. Storetvedt ³⁴, P. Stratmann ¹³⁵, S. Strazzi ²⁵, C.P. Stylianidis ⁸³, A.A.P. Suáide ¹⁰⁹, C. Suire ¹²⁸, M. Sukhanov ¹⁴⁰, M. Suljic ³², V. Sumberia ⁹⁰, S. Sumowidagdo ⁸¹, S. Swain ⁶⁰, I. Szarka ¹², U. Tabassam ¹³, S.F. Taghavi ⁹⁵, G. Taillepied ⁹⁷, J. Takahashi ¹¹⁰, G.J. Tambave ²⁰, S. Tang ^{124,6}, Z. Tang ¹¹⁷, J.D. Tapia Takaki ¹¹⁵, N. Tapus ¹²³, L.A. Tarasovicova ¹³⁵, M.G. Tarzila ⁴⁵, G.F. Tassielli ³¹, A. Tauro ³², A. Telesca ³², L. Terlizzi ²⁴, C. Terrevoli ¹¹³, G. Tersimonov ³, D. Thomas ¹⁰⁷, A. Tikhonov ¹⁴⁰, A.R. Timmins ¹¹³, M. Tkacik ¹⁰⁵, T. Tkacik ¹⁰⁵, A. Toia ⁶³, R. Tokumoto ⁹², N. Topilskaya ¹⁴⁰, M. Toppi ⁴⁸, F. Torales-Acosta ¹⁸, T. Tork ¹²⁸, A.G. Torres Ramos ³¹, A. Trifiró ^{30,52}, A.S. Triolo ^{30,52}, S. Tripathy ⁵⁰, T. Tripathy ⁴⁶, S. Trogolo ³², V. Trubnikov ³, W.H. Trzaska ¹¹⁴, T.P. Trzciński ¹³³, R. Turrisi ⁵³, T.S. Tveter ¹⁹, K. Ullaland ²⁰, B. Ulukutlu ⁹⁵, A. Uras ¹²⁵, M. Urioni ^{54,131}, G.L. Usai ²², M. Vala ³⁷, N. Valle ²¹, S. Vallero ⁵⁵, L.V.R. van Doremalen ⁵⁸, M. van Leeuwen ⁸³, C.A. van Veen ⁹⁴, R.J.G. van Weelden ⁸³, P. Vande Vyvre ³², D. Varga ¹³⁶, Z. Varga ¹³⁶, M. Varga-Kofarago ¹³⁶, M. Vasileiou ⁷⁷, A. Vasiliev ¹⁴⁰, O. Vázquez Doce ⁴⁸, O. Vázquez Rueda ⁷⁴, V. Vechernin ¹⁴⁰, E. Vercellin ²⁴, S. Vergara Limón ⁴⁴, L. Vermunt ⁹⁷, R. Vértesi ¹³⁶, M. Verweij ⁵⁸, L. Vickovic ³³, Z. Vilakazi ¹²⁰, O. Villalobos Baillie ¹⁰⁰, G. Vino ⁴⁹, A. Vinogradov ¹⁴⁰, T. Virgili ²⁸, V. Vislavicius ⁸², A. Vodopjanov ¹⁴¹, B. Volkel ³², M.A. Völkli ⁹⁴, K. Voloshin ¹⁴⁰, S.A. Voloshin ¹³⁴, G. Volpe ³¹, B. von Haller ³², I. Vorobyev ⁹⁵, N. Vozniuk ¹⁴⁰, J. Vrláková ³⁷, B. Wagner ²⁰, C. Wang ³⁹, D. Wang ³⁹, M. Weber ¹⁰², A. Wegrzynek ³², F.T. Weiglhofer ³⁸, S.C. Wenzel ³², J.P. Wessels ¹³⁵, S.L. Weyhmiller ¹³⁷, J. Wiechula ⁶³, J. Wikne ¹⁹, G. Wilk ⁷⁸, J. Wilkinson ⁹⁷, G.A. Willems ¹³⁵, B. Windelband ⁹⁴, M. Winn ¹²⁷, J.R. Wright ¹⁰⁷, W. Wu ³⁹, Y. Wu ¹¹⁷, R. Xu ⁶, A. Yadav ⁴², A.K. Yadav ¹³², S. Yalcin ⁷¹, Y. Yamaguchi ⁹², K. Yamakawa ⁹², S. Yang ²⁰, S. Yano ⁹², Z. Yin ⁶, I.-K. Yoo ¹⁶, J.H. Yoon ⁵⁷, S. Yuan ²⁰, A. Yuncu ⁹⁴, V. Zaccolo ²³, C. Zampolli ³², H.J.C. Zanolli ⁵⁸,

F. Zanone ⁹⁴, N. Zardoshti ^{32,100}, A. Zarochentsev ¹⁴⁰, P. Závada ⁶¹, N. Zaviyalov ¹⁴⁰, M. Zhalov ¹⁴⁰, B. Zhang ⁶, S. Zhang ³⁹, X. Zhang ⁶, Y. Zhang ¹¹⁷, Z. Zhang ⁶, M. Zhao ¹⁰, V. Zherebchevskii ¹⁴⁰, Y. Zhi ¹⁰, N. Zhigareva ¹⁴⁰, D. Zhou ⁶, Y. Zhou ⁸², J. Zhu ^{97,6}, Y. Zhu ⁶, G. Zinovjev^{I,3}, N. Zurlo ^{131,54}

Affiliation Notes

^I Deceased

^{II} Also at: Max-Planck-Institut für Physik, Munich, Germany

^{III} Also at: Italian National Agency for New Technologies, Energy and Sustainable Economic Development (ENEA), Bologna, Italy

^{IV} Also at: Dipartimento DET del Politecnico di Torino, Turin, Italy

^V Also at: Department of Applied Physics, Aligarh Muslim University, Aligarh, India

^{VI} Also at: Institute of Theoretical Physics, University of Wroclaw, Poland

^{VII} Also at: An institution covered by a cooperation agreement with CERN

Collaboration Institutes

¹ A.I. Alikhanyan National Science Laboratory (Yerevan Physics Institute) Foundation, Yerevan, Armenia

² AGH University of Krakow, Cracow, Poland

³ Bogolyubov Institute for Theoretical Physics, National Academy of Sciences of Ukraine, Kiev, Ukraine

⁴ Bose Institute, Department of Physics and Centre for Astroparticle Physics and Space Science (CAPSS), Kolkata, India

⁵ California Polytechnic State University, San Luis Obispo, California, United States

⁶ Central China Normal University, Wuhan, China

⁷ Centro de Aplicaciones Tecnológicas y Desarrollo Nuclear (CEADEN), Havana, Cuba

⁸ Centro de Investigación y de Estudios Avanzados (CINVESTAV), Mexico City and Mérida, Mexico

⁹ Chicago State University, Chicago, Illinois, United States

¹⁰ China Institute of Atomic Energy, Beijing, China

¹¹ Chungbuk National University, Cheongju, Republic of Korea

¹² Comenius University Bratislava, Faculty of Mathematics, Physics and Informatics, Bratislava, Slovak Republic

¹³ COMSATS University Islamabad, Islamabad, Pakistan

¹⁴ Creighton University, Omaha, Nebraska, United States

¹⁵ Department of Physics, Aligarh Muslim University, Aligarh, India

¹⁶ Department of Physics, Pusan National University, Pusan, Republic of Korea

¹⁷ Department of Physics, Sejong University, Seoul, Republic of Korea

¹⁸ Department of Physics, University of California, Berkeley, California, United States

¹⁹ Department of Physics, University of Oslo, Oslo, Norway

²⁰ Department of Physics and Technology, University of Bergen, Bergen, Norway

²¹ Dipartimento di Fisica, Università di Pavia, Pavia, Italy

²² Dipartimento di Fisica dell'Università and Sezione INFN, Cagliari, Italy

²³ Dipartimento di Fisica dell'Università and Sezione INFN, Trieste, Italy

²⁴ Dipartimento di Fisica dell'Università and Sezione INFN, Turin, Italy

²⁵ Dipartimento di Fisica e Astronomia dell'Università and Sezione INFN, Bologna, Italy

²⁶ Dipartimento di Fisica e Astronomia dell'Università and Sezione INFN, Catania, Italy

²⁷ Dipartimento di Fisica e Astronomia dell'Università and Sezione INFN, Padova, Italy

²⁸ Dipartimento di Fisica ‘E.R. Caianiello’ dell’Università and Gruppo Collegato INFN, Salerno, Italy

²⁹ Dipartimento DISAT del Politecnico and Sezione INFN, Turin, Italy

³⁰ Dipartimento di Scienze MIFT, Università di Messina, Messina, Italy

³¹ Dipartimento Interateneo di Fisica ‘M. Merlin’ and Sezione INFN, Bari, Italy

³² European Organization for Nuclear Research (CERN), Geneva, Switzerland

³³ Faculty of Electrical Engineering, Mechanical Engineering and Naval Architecture, University of Split, Split, Croatia

³⁴ Faculty of Engineering and Science, Western Norway University of Applied Sciences, Bergen, Norway

³⁵ Faculty of Nuclear Sciences and Physical Engineering, Czech Technical University in Prague, Prague, Czech Republic

³⁶ Faculty of Physics, Sofia University, Sofia, Bulgaria

- ³⁷ Faculty of Science, P.J. Šafárik University, Košice, Slovak Republic
³⁸ Frankfurt Institute for Advanced Studies, Johann Wolfgang Goethe-Universität Frankfurt, Frankfurt, Germany
³⁹ Fudan University, Shanghai, China
⁴⁰ Gangneung-Wonju National University, Gangneung, Republic of Korea
⁴¹ Gauhati University, Department of Physics, Guwahati, India
⁴² Helmholtz-Institut für Strahlen- und Kernphysik, Rheinische Friedrich-Wilhelms-Universität Bonn, Bonn, Germany
⁴³ Helsinki Institute of Physics (HIP), Helsinki, Finland
⁴⁴ High Energy Physics Group, Universidad Autónoma de Puebla, Puebla, Mexico
⁴⁵ Horia Hulubei National Institute of Physics and Nuclear Engineering, Bucharest, Romania
⁴⁶ Indian Institute of Technology Bombay (IIT), Mumbai, India
⁴⁷ Indian Institute of Technology Indore, Indore, India
⁴⁸ INFN, Laboratori Nazionali di Frascati, Frascati, Italy
⁴⁹ INFN, Sezione di Bari, Bari, Italy
⁵⁰ INFN, Sezione di Bologna, Bologna, Italy
⁵¹ INFN, Sezione di Cagliari, Cagliari, Italy
⁵² INFN, Sezione di Catania, Catania, Italy
⁵³ INFN, Sezione di Padova, Padova, Italy
⁵⁴ INFN, Sezione di Pavia, Pavia, Italy
⁵⁵ INFN, Sezione di Torino, Turin, Italy
⁵⁶ INFN, Sezione di Trieste, Trieste, Italy
⁵⁷ Inha University, Incheon, Republic of Korea
⁵⁸ Institute for Gravitational and Subatomic Physics (GRASP), Utrecht University/Nikhef, Utrecht, Netherlands
⁵⁹ Institute of Experimental Physics, Slovak Academy of Sciences, Košice, Slovak Republic
⁶⁰ Institute of Physics, Homi Bhabha National Institute, Bhubaneswar, India
⁶¹ Institute of Physics of the Czech Academy of Sciences, Prague, Czech Republic
⁶² Institute of Space Science (ISS), Bucharest, Romania
⁶³ Institut für Kernphysik, Johann Wolfgang Goethe-Universität Frankfurt, Frankfurt, Germany
⁶⁴ Instituto de Ciencias Nucleares, Universidad Nacional Autónoma de México, Mexico City, Mexico
⁶⁵ Instituto de Física, Universidade Federal do Rio Grande do Sul (UFRGS), Porto Alegre, Brazil
⁶⁶ Instituto de Física, Universidad Nacional Autónoma de México, Mexico City, Mexico
⁶⁷ iThemba LABS, National Research Foundation, Somerset West, South Africa
⁶⁸ Jeonbuk National University, Jeonju, Republic of Korea
⁶⁹ Johann-Wolfgang-Goethe Universität Frankfurt Institut für Informatik, Fachbereich Informatik und Mathematik, Frankfurt, Germany
⁷⁰ Korea Institute of Science and Technology Information, Daejeon, Republic of Korea
⁷¹ KTO Karatay University, Konya, Turkey
⁷² Laboratoire de Physique Subatomique et de Cosmologie, Université Grenoble-Alpes, CNRS-IN2P3, Grenoble, France
⁷³ Lawrence Berkeley National Laboratory, Berkeley, California, United States
⁷⁴ Lund University Department of Physics, Division of Particle Physics, Lund, Sweden
⁷⁵ Nagasaki Institute of Applied Science, Nagasaki, Japan
⁷⁶ Nara Women's University (NWU), Nara, Japan
⁷⁷ National and Kapodistrian University of Athens, School of Science, Department of Physics , Athens, Greece
⁷⁸ National Centre for Nuclear Research, Warsaw, Poland
⁷⁹ National Institute of Science Education and Research, Homi Bhabha National Institute, Jatni, India
⁸⁰ National Nuclear Research Center, Baku, Azerbaijan
⁸¹ National Research and Innovation Agency - BRIN, Jakarta, Indonesia
⁸² Niels Bohr Institute, University of Copenhagen, Copenhagen, Denmark
⁸³ Nikhef, National institute for subatomic physics, Amsterdam, Netherlands
⁸⁴ Nuclear Physics Group, STFC Daresbury Laboratory, Daresbury, United Kingdom
⁸⁵ Nuclear Physics Institute of the Czech Academy of Sciences, Husinec-Řež, Czech Republic
⁸⁶ Oak Ridge National Laboratory, Oak Ridge, Tennessee, United States
⁸⁷ Ohio State University, Columbus, Ohio, United States
⁸⁸ Physics department, Faculty of science, University of Zagreb, Zagreb, Croatia
⁸⁹ Physics Department, Panjab University, Chandigarh, India

- ⁹⁰ Physics Department, University of Jammu, Jammu, India
⁹¹ Physics Department, University of Rajasthan, Jaipur, India
⁹² Physics Program and International Institute for Sustainability with Knotted Chiral Meta Matter (SKCM2), Hiroshima University, Hiroshima, Japan
⁹³ Physikalisches Institut, Eberhard-Karls-Universität Tübingen, Tübingen, Germany
⁹⁴ Physikalisches Institut, Ruprecht-Karls-Universität Heidelberg, Heidelberg, Germany
⁹⁵ Physik Department, Technische Universität München, Munich, Germany
⁹⁶ Politecnico di Bari and Sezione INFN, Bari, Italy
⁹⁷ Research Division and ExtreMe Matter Institute EMMI, GSI Helmholtzzentrum für Schwerionenforschung GmbH, Darmstadt, Germany
⁹⁸ Saga University, Saga, Japan
⁹⁹ Saha Institute of Nuclear Physics, Homi Bhabha National Institute, Kolkata, India
¹⁰⁰ School of Physics and Astronomy, University of Birmingham, Birmingham, United Kingdom
¹⁰¹ Sección Física, Departamento de Ciencias, Pontificia Universidad Católica del Perú, Lima, Peru
¹⁰² Stefan Meyer Institut für Subatomare Physik (SMI), Vienna, Austria
¹⁰³ SUBATECH, IMT Atlantique, Nantes Université, CNRS-IN2P3, Nantes, France
¹⁰⁴ Suranaree University of Technology, Nakhon Ratchasima, Thailand
¹⁰⁵ Technical University of Košice, Košice, Slovak Republic
¹⁰⁶ The Henryk Niewodniczanski Institute of Nuclear Physics, Polish Academy of Sciences, Cracow, Poland
¹⁰⁷ The University of Texas at Austin, Austin, Texas, United States
¹⁰⁸ Universidad Autónoma de Sinaloa, Culiacán, Mexico
¹⁰⁹ Universidade de São Paulo (USP), São Paulo, Brazil
¹¹⁰ Universidade Estadual de Campinas (UNICAMP), Campinas, Brazil
¹¹¹ Universidade Federal do ABC, Santo Andre, Brazil
¹¹² University of Cape Town, Cape Town, South Africa
¹¹³ University of Houston, Houston, Texas, United States
¹¹⁴ University of Jyväskylä, Jyväskylä, Finland
¹¹⁵ University of Kansas, Lawrence, Kansas, United States
¹¹⁶ University of Liverpool, Liverpool, United Kingdom
¹¹⁷ University of Science and Technology of China, Hefei, China
¹¹⁸ University of South-Eastern Norway, Kongsberg, Norway
¹¹⁹ University of Tennessee, Knoxville, Tennessee, United States
¹²⁰ University of the Witwatersrand, Johannesburg, South Africa
¹²¹ University of Tokyo, Tokyo, Japan
¹²² University of Tsukuba, Tsukuba, Japan
¹²³ University Politehnica of Bucharest, Bucharest, Romania
¹²⁴ Université Clermont Auvergne, CNRS/IN2P3, LPC, Clermont-Ferrand, France
¹²⁵ Université de Lyon, CNRS/IN2P3, Institut de Physique des 2 Infinis de Lyon, Lyon, France
¹²⁶ Université de Strasbourg, CNRS, IPHC UMR 7178, F-67000 Strasbourg, France, Strasbourg, France
¹²⁷ Université Paris-Saclay, Centre d'Etudes de Saclay (CEA), IRFU, Département de Physique Nucléaire (DPhN), Saclay, France
¹²⁸ Université Paris-Saclay, CNRS/IN2P3, IJCLab, Orsay, France
¹²⁹ Università degli Studi di Foggia, Foggia, Italy
¹³⁰ Università del Piemonte Orientale, Vercelli, Italy
¹³¹ Università di Brescia, Brescia, Italy
¹³² Variable Energy Cyclotron Centre, Homi Bhabha National Institute, Kolkata, India
¹³³ Warsaw University of Technology, Warsaw, Poland
¹³⁴ Wayne State University, Detroit, Michigan, United States
¹³⁵ Westfälische Wilhelms-Universität Münster, Institut für Kernphysik, Münster, Germany
¹³⁶ Wigner Research Centre for Physics, Budapest, Hungary
¹³⁷ Yale University, New Haven, Connecticut, United States
¹³⁸ Yonsei University, Seoul, Republic of Korea
¹³⁹ Zentrum für Technologie und Transfer (ZTT), Worms, Germany
¹⁴⁰ Affiliated with an institute covered by a cooperation agreement with CERN
¹⁴¹ Affiliated with an international laboratory covered by a cooperation agreement with CERN.